Aus der

Klinik und Poliklinik für Strahlentherapie und Radioonkologie

LMU Klinikum

Ludwig-Maximilians-Universität München

Direktor: Prof. Dr. med. Claus Belka

Image-guided adaptive photon and proton radiotherapy

Habilitationsschrift zur Erlangung der Venia Legendi im Fach

Experimentelle Strahlentherapie

vorgelegt von

Dr. rer. nat. Christopher Kurz

München 2021

This cumulative habilitation is primarily based on the following peer-reviewed scientific contributions (in the order of appearance in this thesis):

1. **Kurz C**, Dedes G, Resch A, Reiner M, Ganswindt U, Nijhuis R, Thieke C, Belka C, Parodi K, Landry G. Comparing cone-beam CT intensity correction methods for dose calculation in adaptive intensity modulated photon and proton therapy for head and neck cancer. Acta Oncol. 2015;54(9):1651-7. DOI: 10.3109/0284186X.2015.1061206

2. **Kurz C**, Kamp F, Park YK, Zöllner C, Rit S, Hansen DC, Podesta M, Sharp GC, Li M, Reiner M, Hofmaier J, Neppl S, Thieke C, Nijhuis R, Ganswindt U, Belka C, Winey BA, Parodi K, Landry G. Investigating deformable image registration and scatter correction for CBCT-based dose calculation in adaptive IMPT. Med Phys. 2016;43(10):5635-46. DOI: 10.1118/1.4962933

3. Hansen DC, Landry G, Kamp F, Li M, Belka C, Parodi K, **Kurz C**. ScatterNet: a convolutional neural network for cone-beam CT intensity correction. Med Phys. 2018;45(11):4916-26. DOI: 10.1002/mp.13175

4. **Kurz C**, Landry G, Resch A, Dedes G, Kamp F, Ganswindt U, Belka C, Raaymakers BW, Parodi K. A Monte-Carlo study to assess the effect of 1.5T magnetic fields on the overall robustness of pencil-beam scanning proton radiotherapy plans for prostate cancer. Phys Med Biol. 2017;62(21):8470-82. DOI: 10.1088/1361-6560/aa8de9

5. Maspero M, van den Berg CAT, Landry G, Belka C, Parodi K, Seevinck PR, Raaymakers BW, **Kurz C**. Feasibility of MR-only proton dose calculations for prostate cancer radiotherapy using a commercial pseudo-CT generation method. Phys Med Biol. 2017;62(24):9159-76. DOI: 10.1088/1361-6560/aa9677

6. Haehnle J, Süss P, Landry G, Teichert K, Hille L, Hofmaier J, Nowak D, Kamp F, Reiner M, Thieke C, Ganswindt U, Belka C, Parodi K, Küfer KH, **Kurz C**. A novel method for interactive multi-objective dose-guided patient positioning. Phys Med Biol. 2017;62(1):165-85. DOI: 10.1088/1361-6560/62/1/165

Table of contents

1 Introduction and background 3

2 Own scientific contributions 8

2.1 CBCT-guided adaptive radiotherapy 8

2.1.1 Comparing cone-beam CT intensity correction methods for dose calculation in adaptive intensity modulated photon and proton therapy for head and neck cancer 8

2.1.2 Investigating deformable image registration and scatter correction for CBCT-based dose calculation in adaptive IMPT 9

2.1.3 ScatterNet: a convolutional neural network for cone-beam CT intensity correction 10

2.1.4 Further publications related to CBCT-guided adaptive radiotherapy 11

2.2 MRI-guided adaptive proton therapy 12

2.2.1 A Monte-Carlo study to assess the effect of 1.5T magnetic fields on the overall robustness of pencil-beam scanning proton radiotherapy plans for prostate cancer 12

2.2.2 Feasibility of MR-only proton dose calculations for prostate cancer radiotherapy using a commercial pseudo-CT generation method 13

2.2.3 Further publications related to MRI-guided adaptive radiotherapy 14

2.3 Dose-guided patient positioning 15

2.3.1 A novel method for interactive multi-objective dose-guided patient positioning 15

2.3.2 Further publications related to dose-guided patient positioning 16

3 Conclusions and outlook 17

4 List of abbreviations 19

5 Literature 20

6 Acknowledgements 24

7 Declaration 25

8 Facsimile of relevant scientific contributions 26

1 Introduction and background

In Germany close to 500,000 new patients are diagnosed with cancer every year [44]. Therapeutic options comprise surgery, chemo- and targeted therapy, as well as radiotherapy. In total, more than half of all cancer patients undergo radiotherapy as part of their treatment, with the ultimate goal of sterilizing all cancer cells by local energy or dose deposition by ionizing radiation. While the dose to the target volume should be high enough to achieve this aim, the dose to all relevant organs-at-risk (OAR), should be as low as reasonably possible to prevent severe side effects. In most cases, patients follow the workflow illustrated in figure 1.

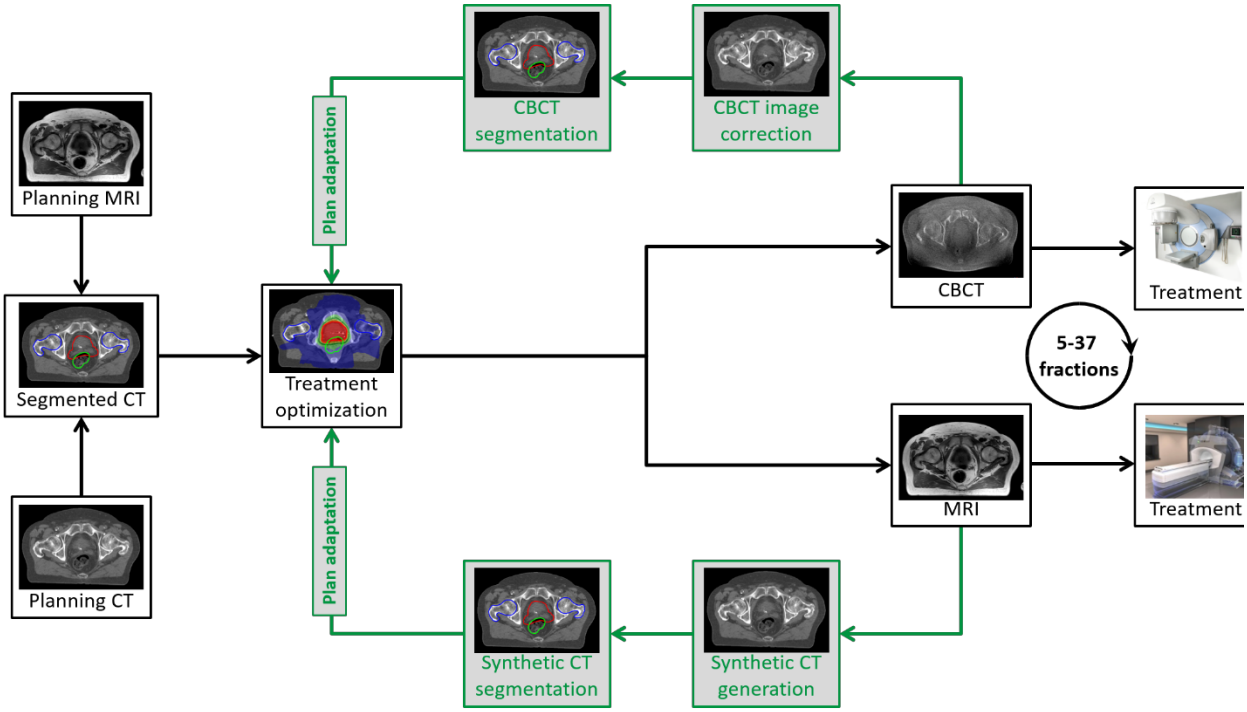

Figure 1. Overview of the typical radiotherapy workflow: Prior to treatment, a planning CT (mandatory for dose calculation during treatment planning) is acquired. Besides, MRI is frequently used for accurate tumor and OAR delineation due to its superior soft-tissue contrast. The segmented CT is then used for treatment optimization with a dedicated planning system. Several days to weeks later, the patient receives the first irradiation fraction. In-room imaging with the patient in treatment position (cone-beam CT (CBCT) or, more recently, MRI) is used for accurate patient alignment. In adaptive radiotherapy, the acquired in-room imaging data is not only used for patient set-up, but also for daily adaptation of the treatment to the actual patient anatomy. For this, the in-room imaging data have to be rendered suitable for accurate dose calculation (CBCT correction or synthetic CT (sCT) generation) and all relevant structures for treatment planning have to be segmented (green).

In modern radiotherapy, image-guidance using various imaging modalities plays an integral role during treatment planning, as well as during patient treatment itself (in-room imaging). At treatment planning stage, an X-ray computed tomography (CT) image is generally acquired in order to derive electron density (photon therapy) or relative stopping power ratio (proton therapy) information, which are required for accurate dose calculation during treatment plan optimization. More and more, CT imaging is accompanied by magnetic resonance imaging (MRI) and/or positron emission tomography (PET) scans. While MRI is typically used to infer more detailed anatomical features for improved tumor and OAR delineation due to its superior soft-tissue contrast, it is more recently also applied to determine functional properties of the

tumor, e.g., by means of diffusion-weighted imaging (DWI) [48]. Also PET imaging aims at determining functional and metabolic properties of tumor tissues, such as glucose uptake rates or oxygenation levels, as well as at identifying potential spread to adjacent lymph nodes or even distant metastasis [21]. Information derived from functional imaging, using either MRI or PET, can then be used for treatment plan personalization, e.g., by defining certain regions in the tumor to receive a higher (boosted) dose level [8]. However, tissue properties derived from functional imaging might not only be considered at treatment planning stage, but also allow for early response assessment in radiotherapy by monitoring their behavior as a function of time during the course of fractionated radiotherapy [22].

Besides the previously described imaging taking place outside the treatment room, mostly at treatment planning stage, in-room imaging [20], aiming at the exact alignment of the patient with respect to the treatment unit, constitutes an indispensable part of image-guided radiotherapy. In combination with modern external beam radiotherapy techniques, such as intensity-modulated photon or proton radiotherapy (IMRT [52], IMPT [9]), in-room imaging theoretically enables tight adjustment of the delivered dose to the target. However, the full potential of these techniques is currently not exploited in clinical practice. The reason for this, and generally one of the major challenges in modern radiotherapy, is the presence of anatomical changes, occurring on time scales from seconds (lung), to minutes (abdomen and pelvis), days or weeks (head and neck [H&N]) [5, 26]. For the vast majority of patients in today's radiotherapy, such anatomical alterations are only considered by introducing safety margins around the actual tumor volume during treatment planning [50]. This ensures irradiation of the tumor to the prescribed dose, but increases the irradiated volume, the dose burden to OARs, and eventually limits the applicable dose and hereby the treatment efficacy. A substantially improved treatment for tumor entities affected by anatomical changes during fractionated radiotherapy, such as H&N, prostate or pancreatic cancer, can be realized by online adaptive radiotherapy (ART) [54]. Instead of applying the same irradiation plan throughout the entire course of treatment (typically several weeks) and assuming the initial planning anatomy is still valid, the treatment is optimized at each irradiation session on basis of the daily anatomy in treatment position, as inferred directly from in-room imaging (figure 1). This intrinsically accounts for anatomical changes and allows for reduced margins and optimal OAR sparing at each fraction, even when increasing the target dose at the same time.

Despite the anticipated benefits, the fraction of patients currently irradiated in online adaptive scenarios is still negligible. The main reason is that nearly all patients in photon and proton radiotherapy are treated using cone-beam CT (CBCT) for in-room imaging. Although CBCT allows for accurate patient alignment, the image quality is hampered by the detection of scattered photons and not sufficient for accurate dose calculation, which is indispensable for treatment adaptation. In the last years, various methods have been proposed for CBCT image correction, aiming at rendering the data suitable for photon and proton therapy dose calculation [12, 30, 39, 41]. Suggested techniques range from simple look-up-table (LUT)-based recalibration of the CT numbers, over CT-to-CBCT deformable image registration (DIR) to more sophisticated projection-based correction algorithms. However, most of them either lack accuracy (LUT-based), robustness (DIR-based) or speed (projection-based) for online application. Only recently, deep learning approaches, in particular convolutional neural networks (CNN), which had already shown impressive results for a variety of medical image processing tasks [3, 11], have been adopted in the context

of CBCT correction. Several groups have reported promising results in terms of correction speed and accuracy utilizing U-shaped CNNs (Unets) [23, 32, 45] or generative adversarial networks (GAN) [13, 17]. These networks enable CBCT intensity correction with accuracy similar to previously published methods, but with correction times of only few seconds once the network models are trained. In the scope of this habilitation, CBCT intensity correction, aiming at yielding images suitable for accurate photon and proton dose calculation in the context of adaptive radiotherapy, was a major focus. Various conventional (LUT-, DIR-, projection-based) and deep learning-based (Unet, GAN) methods have been investigated in terms of their dosimetric accuracy and capability for online application. A detailed description of these works will be given in section 2.1.

Besides the poor image quality, including a comparably low soft-tissue contrast, an important obstacle for CBCT-guided online ART is the imaging dose, which can amount to a total of 1-2 Gy (therapeutic doses: 50 to 70 Gy) if daily imaging is performed for 30 or more fractions [2]. Thus, CBCTs are often acquired less frequently, e.g., only once per week, for treatment sites such as the head and neck region, where anatomical changes are expected to be gradual and occurring over longer time scales.

Due to these limitations of CBCT image-guidance, great efforts have been made over the last decades to realize the integration of MRI as in-room imaging modality. Substantial technical challenges related to the electro-magnetic decoupling and, hereby, interference-free side-by-side operation of the MRI and the treatment machine, had to be overcome. Thus, only during the last few years, integrated MR-linear accelerators (MR-Linacs) became certified and clinically available at few academic institutions. Ever since, this technique has aroused considerable interest in the radiotherapy community [28]. The superior soft-tissue contrast allows for accurate visualization of targets and OARs at no imaging dose, and the vendors of both certified MR-Linacs (ViewRay MRIdian [36] and Elekta Unity [29]) have implemented basic online ART workflows for the first time in the history of radiotherapy [1, 6, 43, 53], leading to a paradigm shift in patient treatment. Besides pre-treatment adaptation, in-room MRI allows for continuous imaging (in 2D) and tracking of the tumor volume itself without requiring any external surrogate [51]. In combination with gated beam delivery, i.e., irradiating only when the target is in a pre-defined location, highly accurate irradiation of tumors affected by intra-fractional motion is feasible. Promising clinical results, among others for pancreatic cancer, have been reported in initial studies [46]. Worldwide, a large number of studies on MRI-guided radiotherapy are still being carried in order to assess the promised clinical benefits from these devices and from online ART workflows.

Due to the substantial personnel, technical and financial outlay of this emerging technique, however, only three MR-Linacs will be installed in Germany by the end of 2020, including an MRIdian MR-Linac at the LMU Department of Radiation Oncology that went clinically operational in January 2020. Worldwide the number of devices is still below one hundred. Additionally, treatments are still limited to entities, such as the prostate or the pancreas, which allow for hypo-fractionated schemes (<10 fractions with higher doses) due to the time overhead of current clinical online adaptive workflows (30-60 minutes per fraction) with respect to conventional radiotherapy (10-20 minutes per fraction). Thus, despite the foreseen potential of these new machines in the future, more efficient clinical routines and workflows will have to be developed.

Nevertheless, recently also interest in combining the advantages of MRI-guidance and proton therapy, currently relying on CBCT as in-room imaging modality, is growing in the radiotherapy community [40]. In proton therapy, even larger benefits are anticipated from ART due to the higher sensitivity of proton dose distributions to anatomical changes [24], which might be substantially reduced when using MR-guidance. Also considering the potentially advantageous proton dose distributions allowing for considerably reduced integral dose, MR-guided proton therapy has the potential to further boost treatment efficiency in radiotherapy in the future. A first pre-clinical prototype has just lately been installed in Dresden and technical feasibility studies are on-going [47]. Similar to photon therapy, a major challenge is to electro-magnetically decouple the MRI scanner and the beam delivery system. Taking into the consideration that up-to-date proton therapy facilities utilize pencil-beam scanning dose delivery with magnetic steering of the beam, it can be acknowledged that substantial technical issues will have to be solved to pave the way towards clinical implementation. On top, and in contrast to MRI-guided photon therapy, also the impact of the MRI scanner B-fields on the treatment beam itself has to be carefully modeled and considered during treatment planning. In the scope of this habilitation, the first study on the feasibility of fully inverse IMPT optimization in B-fields has been conducted. Moreover, the obtained plans have been investigated in depth in terms of their robustness against anatomical and positional uncertainties. The corresponding publication will be described in more detail in section 2.2.

Another main challenge MRI-guided ART with photons, as well as potentially in the future with protons, is facing, is the conversion of the in-situ in-room MRIs into synthetic CTs (sCT). These are required for accurate dose calculation and adaptation since the MRI signal cannot be directly converted into the required electron density or stopping power ratio information [10]. Today, both vendors of clinically certified MR-Linacs utilize an initial planning CT and CT-to-MRI DIR for sCT generation [6, 53]. But, DIR accuracy is often limited in regions with pronounced inter-fractional anatomical changes, such as the abdomen or pelvis, where the largest benefits from ART are actually anticipated. More accurate, fully automatic and rapid sCT generation for MRI-guided online ART might in the future be achieved by deep learning. Unets, and also GANs [13], have been shown to yield sCTs suitable for accurate photon dose calculation [7, 15, 33]. A further advantage of CNNs is that, once trained, no planning CT is required for sCT generation, thus allowing an MR-only workflow that could reduce dose burden to the patient, as well as the clinical workload. However, CNN-based sCT algorithms have not yet been clinically applied in the scope of MRI-guided photon therapy. In proton therapy, even higher CT number accuracy than in photon therapy will be required for sCT generation, given the sensitivity of proton dose calculations to the underlying stopping power maps. Nevertheless, several studies on sCT generation for MRI-guided proton therapy exist and suggest clinically acceptable accuracy for proton dose calculation. The used algorithms are based either on bulk-assignment, on LUT-based approaches [14, 25, 34, 42] or on the utilization of deep learning techniques [31, 37, 49]. In the scope of this habilitation, methods for sCT generation using conventional bulks-assignment techniques, as well as deep CNNs, have been investigated for application in proton, but also in photon therapy. More details will be provided in section 2.2.

Beyond the previously discussed challenges related to CBCT intensity correction and sCT generation for accurate dose calculation, image-guided online ART requires accurate target and OAR delineation for treatment plan optimization. Until today, this remains a manual task requiring a trained physician for tens

of minutes to hours, which is not acceptable for online ART where the patient has to stay on the treatment table. In current clinically implemented MRI-guided photon ART workflows, contours are obtained via the same DIR as the sCT and suffer from the same limited accuracy. Often extensive and time-consuming manual corrections are required, rendering segmentation one of the bottlenecks in MRI-based ART. Various deep learning techniques based on CNNs have, however, shown great potential for fast (<1 min) accurate and fully automatic delineation of MRI data [35, 38] and are anticipated to further streamline the online ART workflow in the future. Similarly, recent studies have demonstrated impressive results for rapid automated contouring of the pelvic and the H&N region on CT images using 3D CNN architectures [4, 19]. So far, these algorithms were mainly restricted to applications using diagnostic CT images, but translation to in-room CBCT images is an active field of research, eventually aiming at clinical implementation of a CBCT-guided ART workflow.

In the scope of this habilitation project, also an alternative to online ART relying on daily re-optimization of the irradiation plan from scratch has been addressed: the so-called dose-guided patient positioning. The main idea behind this approach is to utilize daily in-room imaging data (CBCT or MRI) and up-to-date delineations of all relevant structures to determine the couch shift, which results in the best-possible dosimetric outcome (using the original treatment plan) on the day of treatment. This is anticipated advantageous in comparison to the routinely used bone- or marker-based patient alignment in scenarios with non-rigid anatomical changes, where the initially planned dose distribution cannot be fully restored. In comparison to ART, no new treatment plan has to be generated and thus no online quality-assurance procedure is required. Moreover, the optimal dose-guided shift could be determined by the radiotherapy technicians. Presence of a clinician, who is indispensable for plan approval in ART, is not required. For optimal clinical exploitation and efficiency, dose-guided patient positioning has been implemented as a multi-criteria optimization (MCO) problem with a subspace of Pareto-optimal solutions (i.e., patient shifts), which can be interactively browsed by the user. More details will be given in section 2.3.

To summarize, the research performed in the scope of this habilitation intents to pave the way towards widespread clinical adoption of online adaptive photon and proton radiotherapy. To this aim, the following crucial aspects of online ART have been addressed in detail:

1. CBCT intensity correction to enable accurate photon and proton dose calculation (section 2.1)
2. Synthetic CT generation and treatment planning for MRI-guided proton therapy (section 2.2)
3. Dose-guided patient positioning as alternative to full online plan re-optimization (section 2.3)

An exemplary selection of the correlated peer-reviewed articles will be described in chapter 2, considering especially publications as first or last author in the scope of this habilitation. Facsimiles of these publications can be found in chapter 8.

2 Own scientific contributions

2.1 CBCT-guided adaptive radiotherapy

2.1.1 ***Kurz C****, Dedes G, Resch A, Reiner M, Ganswindt U, Nijhuis R, Thieke C, Belka C, Parodi K, Landry G. Comparing cone-beam CT intensity correction methods for dose calculation in adaptive intensity modulated photon and proton therapy for head and neck cancer. Acta Oncol. 2015;54(9)*

In light of the previously described limitations in CBCT image quality, intensity correction strategies to enable accurate dose calculation for plan adaptation in online ART have been investigated in this study. More specifically, two different correction methods have been evaluated in terms of their dose calculation accuracy for photon and proton radiotherapy of the H&N region. The simpler considered approach was to perform correction via a population-based Hounsfield Unit (HU) rescaling [27]. For this, the HU values on a reference diagnostic CT and a corresponding CBCT were sampled for air (inside and outside the patient), fatty tissue, muscle, brain, soft and hard bone using a cohort of 9 H&N cancer patients. With these pairs of values, a LUT was generated and used for CBCT rescaling. The method was compared to a CT-to-CBCT DIR-based approach (virtual CT [vCT]), using a Morphon's algorithm, which had been suggested in a previous publication [30]. DIR used a metric based on the local image phase, thus focusing on the alignment of edges in moving (CT) and fixed (CBCT) images, which is deemed superior to an intensity-based approach when performing cross-modality image registration. To infer the dosimetric accuracy of both approaches photon and proton treatment plans were recalculated on the obtained corrected CBCTs and compared to a reference dose calculation using a diagnostic quality replanning CT acquired close in time. Dose distributions were compared by means of clinically relevant dose-volume-histogram (DVH) parameters and a gamma-index analysis.

While both approaches, LUT and DIR, were found to yield accurate dosimetric results for photon therapy of H&N cancer, the vCT clearly outperformed the LUT-based approach for proton therapy, where higher HU accuracy is required. In particular, the LUT-based approach failed at correcting the CBCT in the area between the shoulders, which is affected by substantial shadowing artifacts. These could not be overcome by using a single LUT for CBCT intensity rescaling.

In a follow-up study, the feasibility of using the more accurate vCT and the corresponding warped structures (target and OARs, using the same CT-to-CBCT deformation field) for automated proton therapy plan adaptation, mimicking an online ART workflow, was investigated [see section 2.1.4, A1]. For the same 9 H&N patients, a novel treatment plan using the vCT and the corresponding structures was generated automatically by using the same treatment planning settings as in the initial planning scenario. The new vCT-based plan was then recalculated on a reference diagnostic replanning CT acquired 30 to 50 days after the initial planning CT (but within 1 to 3 days of the considered CBCT). It could be shown that the automatically obtained vCT-based adapted plans yielded clinically preferable plans on this replanning CT when compared to the initial treatment plan. In particular, hotspots related to patient weight-loss and tumor shrinkage could be efficiently diminished, thus demonstrating for the first time the feasibility of automated, DIR-based online proton ART for H&N cancer.

2.1.2 ***Kurz C****, Kamp F, Park YK, Zöllner C, Rit S, Hansen DC, Podesta M, Sharp GC, Li M, Reiner M, Hofmaier J, Neppl S, Thieke C, Nijhuis R, Ganswindt U, Belka C, Winey BA, Parodi K, Landry G. Investigating deformable image registration and scatter correction for CBCT-based dose calculation in adaptive IMPT. Med Phys. 2016;43(10)*

Since the DIR-based vCT approach could be successfully applied for CBCT correction in photon and proton therapy in the H&N region, this follow-up study aimed at extending it to the pelvic region, considering a cohort of prostate cancer patients. While the H&N region is mostly affected by gradual anatomical changes, e.g., due to patient weight-loss, the pelvis is subject to more pronounced and random inter-fractional changes, e.g., related to variations in bladder and rectum filling. Under these conditions, the DIR approach was found considerably less accurate than observed in the H&N region. In particular, the algorithm failed in accurately modeling large volume changes of the rectum or the bladder, which are typically accompanied by pronounced sliding motion.

Because of this, an alternative CBCT correction technique using the vCT only as a prior to perform projection-based scatter correction [39, 41] was studied as an alternative. In this approach, a forward projection of the vCT using the geometry of the gantry-mounted CBCT scanner is first performed. The contribution of scattered photons, and also of other low-frequency perturbations such as beam hardening [A2], in the measured CBCT projections is then estimated by subtracting the presumably scatter-free vCT forward projections from the measured CBCT projections and applying a generous filter (due to the assumed low spatial frequency). This estimated scatter contribution is then subtracted from the measured CBCT projections, yielding a set of scatter-corrected projections, which can be reconstructed to obtain an intensity corrected CBCT (CBCTcor).

vCT and CBCTcor were compared for two cohorts of H&N and prostate cancer patients. For the H&N cohort, where the vCT had shown to yield dosimetrically accurate results in previous studies, the CBCTcor was found equivalent. Also for the prostate cohort, vCT and CBCTcor obtained almost similar proton dose distributions. However, when carefully checking the geometric fidelity of both images, CBCTcor was found superior for the prostate patients. In particular, as already mentioned above, the vCT yielded incorrectly shaped internal structures, which became apparent in a comparison with the original (uncorrected) CBCT image. In particular, the geometry of the OARs, i.e., of the rectum and the bladder, was found inconsistent. While the impact of these geometric deviations on dose calculation was only minor, they would clearly hamper treatment evaluation and treatment plan optimization (DVH calculation). When looking at CBCTcor, remaining artifacts from the incorrect vCT prior were still visible, but the impact was substantially reduced and accurate delineation of all OARs could be demonstrated.

Given the superior robustness of the CBCTcor approach, it is supposed to be particularly beneficial in regions suffering from pronounced inter-fractional anatomical changes and, thus, reduced DIR accuracy. Both approaches, vCT and CBCTcor, were employed in several further studies described in the following section and listed in section 2.1.4, A1-A6.

*2.1.3 Hansen DC, Landry G, Kamp F, Li M, Belka C, Parodi K, **Kurz C**. ScatterNet: a convolutional neural network for cone-beam CT intensity correction. Med Phys. 2018;45(11)*

Although the CBCTcor intensity correction approach proved to allow for accurate photon and proton dose calculation for different tumor sites, one main drawback of the method is the long processing time, being in the order of 5-7 minutes. Especially when considering its application for online adaptation, with the patient on the treatment table, this is not acceptable. Also due to the fact that, e.g., in the prostate region, anatomical changes can progress on similar time-scales. In this contribution, a potential solution has been investigated: the application of deep CNNs, which have show remarkable performance for many image-to-image translation tasks in recent years and have extremely short application times once the networks are trained.

To this aim, a deep Unet was trained and evaluated in terms of dosimetric accuracy for projection-based intensity correction using clinical CBCT data of 30 prostate cancer patients in this study. The basic idea is depicted in figure 2: The network is trained to translate a measured projection into a scatter corrected projection, as obtained from the accurate, but slow CBCTcor reference method. The output of the network is compared to this reference by means of a loss function (L2 norm in this case) in order to optimize the free parameters of the network iteratively. The network used a conventional Unet design with an encoding (down-sampling) and decoding (up-sampling) branch, linked via so-called skip connections which enable a direct flow of extracted features from the encoding to the decoding branch at each level of the network. Down- and up-sampling blocks made use of so-called residual blocks, i.e., skip connections of convolutional layers, to ease training of the network [18]. In total, 7323 projections of 15 patients were used for training in 2D, using pairs of measured and corrected 2D projections. During training the value of the loss function was monitored for 7 validation patients in order to determine the optimal stopping point for training. Eventually, photon and proton dose calculation accuracy was evaluated for the remaining 8 independent test patients, using CBCTcor as a reference image.

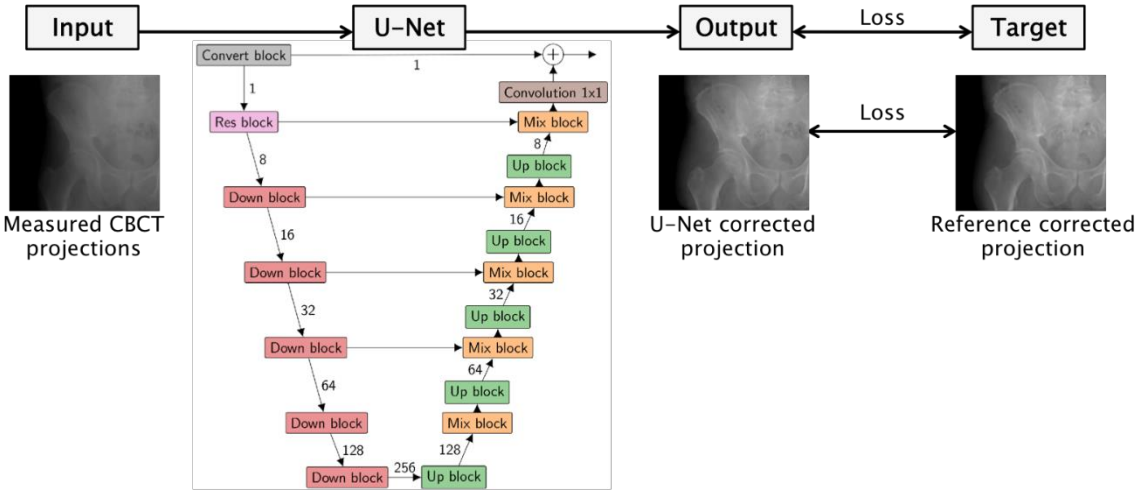

Figure 2. Conceptual design of the Unet investigated for CBCT scatter correction [16]. The network consists of several down- and up-sampling building blocks and aims at translating measured projections into corrected projections. For training, the network output is compared to a reference corrected projection by means of an L2 loss function.

Once the network was trained, which took in the order of 30 to 40 hours, it took only about 0.01 s to correct a single CBCT projection. For a whole CBCT data set, correction can thus be achieved within few seconds, rendering this method particularly interesting in the scope of CBCT-guided online ART. In addition, it was shown that Unet-based CBCT correction is not only fast, but also dosimetrically accurate for photon and proton therapy, yielding dose distributions in close agreement to CBCTcor. Due to using the CBCTcor projections for training, the method was also found robust in the presence of pronounced anatomical changes, e.g., in the bladder.

In a second study on deep learning-based CBCT correction, the versatility of the proposed Unet design for CBCT intensity correction could be demonstrated. The same network was successfully trained to not only perform CBCT correction in projection space, but also in image space [A5]. For this, the network was trained to translate the raw reconstructed CBCT image without applying any corrections into either a vCT or a CBCTcor. For all three training strategies (projections, vCT, CBCTcor), intensity-corrected CBCT images were obtained that allowed for accurate photon and proton dose calculation.

As an alternative network design, a cycle-consistent GAN (cycleGAN) was also investigated for performing CBCT intensity correction in a further study [A6]. The cycleGAN was trained to translate CBCTs into CT equivalent images. GANs are conceptually different from Unets and consist of a generator and a discriminator network, which are trained jointly using an adversarial loss function: while the generator network aims at generating as realistic as possible CT images from input raw CBCT images, the discriminator aims at distinguishing between fake (generator output) and real CT images. By adding a dedicated cycle-consistency loss function for conditioning the generator network outwork on the input, the cycleGAN can be trained using unpaired image data. This is a unique feature for deep CNNs and is feasible due to the fact that the network output is not compared on a pixel-by-pixel basis to a reference image. Unpaired training is deemed of particular interest for applications where matching training data is difficult to obtain, e.g., in the prostate region, where pronounced inter-scan anatomical changes between diagnostic CT and daily CBCT occur. In the respective study, it could be shown for the first time that accurate CBCT correction using a cycleGAN and unpaired training is feasible in the scope of adaptive photon and proton therapy.

2.1.4 Further publications related to CBCT-guided adaptive radiotherapy

A1. **Kurz C**, Nijhuis R, Reiner M, Ganswindt U, Thieke C, Belka C, Parodi K, Landry G. Feasibility of automated proton therapy plan adaptation for head and neck tumors using cone beam CT images. Rad Onc. 2016;11:64

A2. Zöllner C, Rit S, **Kurz C**, Vilches-Freixas G, Kamp F, Dedes G, Belka C, Parodi K, Landry G. Decomposing a prior-CT-based cone-beam CT projection correction algorithm into scatter and beam hardening components. Phys Imag Radiat Oncol (phiRO). 2017;3:49-52

A3. Hofmaier J, Haehnle J, **Kurz C**, Landry G, Maihoefer C, Schüttrumpf L, Süss P, Teichert K, Söhn M, Spahr N, Brachmann C, Weiler F, Thieke C, Küfer KH, Belka C, Parodi K, Kamp F. Multi-criterial patient positioning based on dose recalculation on scatter-corrected CBCT images. Radiother Oncol. 2017;125(3):464-9

A4. Niepel K, Kamp F, **Kurz C**, Hansen DC, Rit S, Neppl S, Hofmaier J, Bondesson D, Thieke C, Dinkel J, Belka C, Parodi K, Landry G. Feasibility of 4DCBCT-based proton dose calculation: an ex-vivo porcine lung phantom study. Z Med Phys. 2019;29(3):249-61

A5. Landry G, Hansen DC, Kamp F, Li M, Hoyle B, Weller J, Parodi K, Belka C, **Kurz C**. Comparing Unet training with three different datasets to correct CBCT images for prostate radiotherapy dose calculations. Phys Med Biol. 2019;64(3):035011

A6. **Kurz C**, Maspero M, Savenije MHF, Landry G, Kamp F, Pinto M, Li M, Parodi K, Belka C, van den Berg CAT. CBCT correction using a cycle-consistent generative adversarial network and unpaired training to enable photon and proton dose calculation. Phys Med Biol. 2019; 64(22):225004

2.2 MRI-guided adaptive proton therapy

*2.2.1 **Kurz C**, Landry G, Resch A, Dedes G, Kamp F, Ganswindt U, Belka C, Raaymakers BW, Parodi K. A Monte-Carlo study to assess the effect of 1.5T magnetic fields on the overall robustness of pencil-beam scanning proton radiotherapy plans for prostate cancer. Phys Med Biol. 2017;62(21)*

Besides CBCT, MRI is playing an increasingly import role for in-room imaging in photon radiotherapy. For its application in proton therapy, as described above, considerable technical challenges remain to be solved before clinical introduction. Nevertheless, similar to photon therapy, proton therapy could greatly benefit from the superior soft-tissue contrast as well as the online real-time imaging capabilities of MRI in comparison to CBCT and is thus gaining interest. In the study described in this section, one of the crucial ingredients for performing MRI-guided proton ART, namely the treatment plan optimization under consideration of the MRI magnetic field, has been addressed.

In contrast to photon therapy, the MRI B-field not only affects the secondary electrons, but also the primary beam particles. In this proof-of-concept study, inverse pencil-beam scanning IMPT planning in the presence of a simplified cylindrical 1.5 T magnetic field perpendicular to the proton beam has been successfully implemented. For the first time also an accurate modeling of the patient geometry in the underlying Monte-Carlo simulations, based on the given patient CT image, was performed. For treatment plan optimization, pencil-beams with Bragg peaks in vicinity of the target volume were first selected and the individual pencil-beam doses calculated under consideration of the B-field using the GEANT4 Monte-Carlo code. To obtain the final treatment plan, the weights of the individual pencil beams were then optimized using an in-house developed research treatment plan optimization tool (CERR).

The implemented treatment planning pipeline was also used to infer the robustness of IMPT plans in the presence of a perpendicular magnetic field. A cohort of 5 prostate cancer patients with 3 repeated CTs each was included in the study. Different orientations of the patients with respect to the magnetic field were considered, just as different gantry angles. Robustness against inter-fractional anatomical changes, as well as robustness against variations in patient set-up (shifts of ±5 mm in anterior-posterior and left-right direction) were studied for the different scenarios and compared to standard IMPT without magnetic field. Results showed that MRI-guided proton therapy is feasible yielding similar plan quality and robustness as found in conventional CT-based proton therapy without magnetic fields. However, to achieve comparable robustness, adaptation of the treatment geometry (in this case of the gantry angle)

was required. The adaptation had to be performed in such a way that the (due to the magnetic deflection) curved proton path within the patient was as close as possible to the proton path in the scenario without magnetic field. For this, an optimal gantry angle of 81°, instead of the clinically used 90° for the given patient set-up, was determined (see figure 3). The reduced robustness observed without gantry angle adaptation (i.e., using an angle of 90°) was related to the fact that the curved proton beam traversed regions which were subject to more pronounced inter-fractional changes related to rectum filling and body outline variations. Thus, for other anatomical sites, adaptation of the gantry angles might have to be performed in a different way, also due to the fact that the curvature of the proton beam will change when using different initial beam energies.

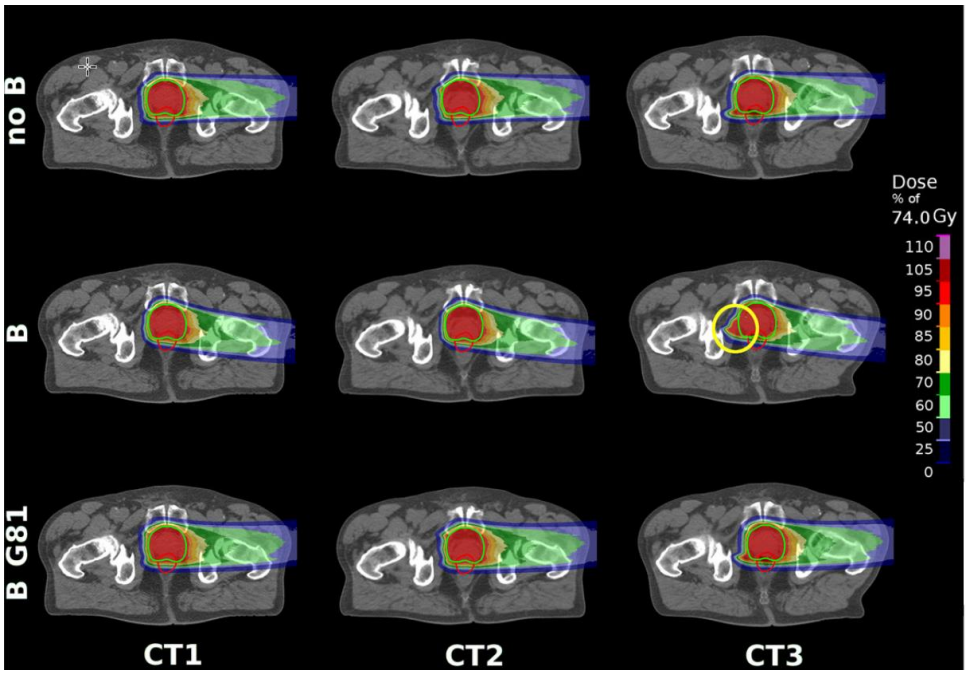

Figure 3. Proton dose distributions for an exemplary prostate patient optimized on CT1 and recalculated on CT2/3 to infer the robustness against inter-fractional anatomical changes for different scenarios: Treatment without B-field (top row), as well as treatment in presence of a 1.5 T B-field perpendicular to the incident beam using gantry angles of 90° (middle row) and 81° (bottom row). Robustness for the B-field scenario with 81° gantry angle was similar to the conventional scenario without B-field, while reduced robustness was observed for a gantry angle of 90° in presence of the B-field. A substantial overshoot on CT 3 is indicated by the yellow circle.

2.2.2 Maspero M, van den Berg CAT, Landry G, Belka C, Parodi K, Seevinck PR, Raaymakers BW, ***Kurz C****. Feasibility of MR-only proton dose calculations for prostate cancer radiotherapy using a commercial pseudo-CT generation method. Phys Med Biol. 2017;62(24)*

Another crucial input required for MRI-guided adaptive proton therapy is the generation of synthetic CT images from in-room MRI for accurate dose calculation. This topic has been investigated in the context of prostate cancer in the study presented in this section. A commercially available and certified photon-oriented solution, called MRCAT (MR for calculating attenuation) has been adapted for application in proton therapy. The method relies on a dual spoiled gradient echo MRI sequence and Dixon reconstruction, in combination with a constrained shape bone model and bulk density assignment of 5 tissue classes (air, fat, muscle, spongy and compact bone) for sCT generation.

In this contribution the method was extended to allow also for the identification of internal gas pockets, which is crucial for accurate proton dose estimation in the pelvis. Moreover, it was found that the used bulk-assigned HU values for spongy and compact bone, which were initially optimized for application in photon therapy, had to be adapted to yield optimal proton dose calculation accuracy. The latter was inferred from recalculating proton plans optimized using diagnostic planning CTs on the MRCAT images and dosimetric comparison. After elimination of inter-scan differences between the planning CT and the MRI used for MRCAT generation, clinically acceptable proton dose calculation accuracy was found, despite the limited number of tissue classes. However, adaptation of the bulk-assigned HU values for bones with respect to the original photon-based solution was found crucial.

In a more recent co-authored paper also the feasibility of using 2D or 3D Unets for MR-only sCT generation in proton therapy was shown for the first time [see section 2.2.3, B1]. The network design was similar to the design used for CBCT correction, as described in section 2.1. In comparison to the MRCAT solution, the Unet approach yields sCTs with a continuous HU range. Overall, good accuracy was found for proton and for photon dose calculation in a cohort of brain tumor patients. In particular, the depp CNN enabled accurate separation of bony anatomy and internal air cavities, which is typically found a major challenge for sCT generation since both structures show no or very low signal on MRI.

Further studies in the field of MRI-guided radiotherapy (with photons and protons) that have been pursued in the scope of this habilitation are listed in section 2.2.3 [B2-B4]. These include two recent review articles on the medical physics challenges of MRI-guided photon therapy and the current status and future perspectives of MRI-guided proton therapy.

2.2.3 Further publications related to MRI-guided adaptive radiotherapy

B1. Neppl S, Landry G, **Kurz C**, Hansen DC, Hoyle B, Stöcklein S, Seidensticker M, Weller J, Belka C, Parodi K, Kamp F. Evaluation of proton and photon dose distributions recalculated on 2D and 3D Unet-generated pseudoCTs from T1-weighted MR head scans. Acta Oncol. 2019;58(10):1429-34

B2. Rabe M, Thieke C, Düsberg M, Neppl S, Gerum S, Reiner M, Nicolay NH, Schlemmer HP, Debus J, Dinkel J, Landry G, Parodi K, Belka C, **Kurz C***, Kamp F*. Real-time 4D-MRI-based internal target volume definition for moving lung tumors. Med Phys. 2020;47(4):1431-42.
*Both authors contributed equally

B3. **Kurz C**, Buizza G, Landry G, Kamp F, Rabe M, Paganelli C, Baroni G, Reiner M, Keall PJ, van den Berg CAT, Riboldi M. Medical physics challenges in clinical MR-guided radiotherapy. Radiat Oncol. 2020;15:93

B4. Hoffmann A, Oborn B, Moteabbed M, Yan S, Bortfeld T, Knopf AC, Fuchs H, Georg D, Seco J, Spadea MF, Jäkel O, **Kurz C**, Parodi K. MR-guided proton therapy: a review and a preview. Radiat Oncol. 2020;15:129

2.3 Dose-guided patient positioning

2.3.1 Haehnle J, Süss P, Landry G, Teichert K, Hille L, Hofmaier J, Nowak D, Kamp F, Reiner M, Thieke C, Ganswindt U, Belka C, Parodi K, Küfer KH, ***Kurz C****. A novel method for interactive multi-objective dose-guided patient positioning. Phys Med Biol. 2017;62(1)*

In this joint project with colleagues at the Fraunhofer Institute for Industrial Mathematics (ITWM) in Kaiserslautern, a prototype software for interactive dose-guided positioning has been implemented and dosimetrically compared to conventional bony anatomy-based alignment for the first time. Dose-guided positioning was technically implemented as an iso-center planning problem (ICPP), which could then be solved under consideration of user-defined clinical objectives, such as DVH parameters for target coverage or OAR dose limits. Since for more than one clinical objective the ICPP is an MCO problem, trading off, e.g., dose to the target against dose to OARs, there is a set of Pareto-optimal solutions. By linear dose-interpolation between different iso-center shifts, the developed tool allows the user to interactively browse through the continuous space of Pareto-optimal patient positions and to straightforwardly determine the clinically optimal patient shift under consideration of the dose.

The efficiency of the approach was demonstrated for 3 H&N and 3 prostate cancer patients using IMRT, following careful validation of the dose interpolation accuracy. A delineated replanning CT was considered as surrogate for the daily in-room image of each patient. In a more realistic scenario, either an intensity corrected CBCT or an MRI-based sCT might be used. In all cases, dose-guided alignment allowed to find a clinically preferable position in comparison to bony anatomy-based alignment. The main effects were an increased target coverage in combination with a reduced dose to the parotid glands (H&N) or the rectum (prostate). However, the study also showed that, in particular for H&N, plan re-optimization, which would in practice be feasible with the same input data (in-room image and segmentation), could achieve even better daily dose distributions.

In a follow-up study, also the applicability of the developed dose-guided positioning tools in the scope of proton therapy has been investigated [see section 2.3.2, C1]. In total 14 H&N and 8 prostate cancer patients with up to 5 repeated CTs were considered. Dose-guided positioning was again compared to the clinically used bony anatomy-based alignment. For the H&N cohort, the main effect of dose-based positioning was a reduction of the dose to the serial organs (spinal cord and brain stem). For the prostate cohort, under-dosage of the target structures could be reduced. Nevertheless, also limitations in the scope of proton therapy were identified. For the H&N cohort, it was not possible to diminish target over-dosage related to patient weight-loss. To properly account for weight-loss, reduction of the initial proton fluence, e.g., in the context of a plan re-optimization, would be necessary.

Since no labor-intensive online quality assurance and plan approval by a certified radiation oncologist is required, dose-guided patient alignment might, nevertheless, still be considered an interesting alternative to full online ART.

2.3.2 Further publications related to dose-guided patient positioning

C1. **Kurz C**, Süss P, Arnsmeyer C, Haehnle J, Teichert K, Landry G, Hofmaier J, Exner F, Hille L, Kamp F, Thieke C, Ganswindt U, Valentini C, Hölscher T, Troost E, Krause M, Belka C, Küfer KH, Parodi K, Richter C. Dose-guided patient positioning in proton therapy using multicriteria-optimization. Z Med Phys. 2019;29(3):216-28

3 Conclusions and outlook

In the scope of this habilitation, studies on various aspects of image-guided adaptive photon and proton therapy have been conducted. Focus was on the ability to render in-room imaging data suitable for accurate daily dose calculation, as required for treatment plan adaptation in an ART workflow. CBCT, as well as MRI, have been considered as the clinically most relevant in-room imaging modalities today. Different methods for the required image correction (CBCT) or translation (MRI to CT) have been investigated, ranging from conventional techniques (LUT-based rescaling, DIR, projection-based correction or bulk assignment) to novel deep learning-based approaches using CNNs (Unet, GAN). In particular, the latter allow for accurate image correction with unparalleled speed and are thus of growing interest in the scope of ART, where time is a crucial factor. Despite the anticipated benefits from deep leaning-based solutions, they are nowadays still restricted to research applications. For future clinical integration, careful safety and risk assessment of these algorithms is indispensable. Major challenges will be posed by the *black-box* nature of neural networks and the fact that trained CNN models typically do not generalize well on unseen data-sets. Thus, it is likely that models will struggle for patients with non-standard anatomies, e.g. due to surgical resection of tissue. How network inaccuracies in such cases can be detected and eventually overcome is still a topic of on-going research.

Beyond image correction for enabling accurate dose calculation, the generation of accurate delineations on the daily in-room imaging data to be used during treatment optimization is a major challenge for online ART. Here, depending on the treatment site, the currently clinically implemented DIR-based approach for MRI-guided photon ART is often facing limitations. Similar observations have been made in the scope of this habilitation in the context of CBCT-based ART. While DIR was found sufficiently accurate for intensity correction and contour propagation to enable automatic treatment plan adaptation in the H&N region, limited accuracy was found in the pelvis. Generally, in the presence of pronounced anatomical changes, DIR-based segmentation will often require time-consuming manual correction by an expert. Unfortunately, exactly these patients, suffering from substantial inter-fractional alterations, are expected to have the largest benefit from online ART. Thus, one important focus of future research is the fast and fully automatic segmentation of in-room imaging data. Similar to image correction, deep learning strategies, often using 3D CNN architectures and dedicated loss metrics (e.g., based on the Dice-similarity coefficient), have shown impressive results for this task, outperforming classical segmentation algorithms, based e.g., on atlases and DIR. First certified deep learning solutions for auto-segmentation of various body sites have recently been launched by different vendors but are still limited to the initial treatment planning stage rather than the online plan adaptation stage using in-room imaging data.

Following image correction or translation and segmentation, online adaptation of the treatment plan becomes feasible. While in photon therapy fast Monte-Carlo dose calculation algorithms taking into consideration the magnetic fields (in the case of MRI-guidance) are used in clinical routine, aspects of proton treatment planning in magnetic fields, as required for clinically realizing MRI-guided proton therapy, have been addressed for the first time in the scope of this habilitation. The feasibility of fully inverse pencil-beam scanning treatment optimization in a magnetic field could be shown, together with the robustness of the generated plans. Although there are still considerable technical hurdles to be

overcome, there is a strongly growing interest in this novel treatment approach. One of the main reasons is that considerable benefits from MRI-guidance for proton therapy are anticipated, since it might help to overcome issues related to the sensitivity of proton therapy to inter- and intra-fractional anatomical changes by providing online treatment adaptation and imaging during beam delivery.

As an alterative approach to daily re-optimization of the treatment plan, MCO-based dose-guided patient positioning has been investigated for photon and for proton therapy in this habilitation. While it requires similar input as online ART, i.e., segmented in-room images suitable for accurate dose calculation, it does require neither online plan quality assurance, nor clinical approval by an expert radiation oncologist. Nevertheless, the daily dose distributions' quality achieved with dose-guided positioning was found inferior to that achieved with plan adaptation from scratch.

While initial online ART workflows using integrated MR-Linacs become more and more widespread, and first certified solutions for CBCT-based ART are lately being introduced by vendors, many challenges remain. These encompass further streamlining the established clinical workflows, in particular by exploiting novel deep learning techniques, but also the extension of treatment adaptation procedures to shorter timescales. More specifically, current workflows only enable adaptation of the treatment with respect to inter-fractional anatomical changes, i.e., once prior to the irradiation, while intra-fractional changes, e.g., related to respiratory motion, are still mitigated by gating, using fast 2D imaging for target tracking in the case of MRI-guidance. In the future, a considerably faster treatment delivery (without beam-off times) could be achieved by implementing real-time ART. For this, a continuous stream of 3D images would be used for real-time accumulation of the already applied dose, followed by prompt adaptation of the remaining treatment. Main challenges to be overcome are the 3D imaging at sufficient frame rates (few Hz), as well as performing accumulation and optimization in real-time. Both aspects are subject of on-going scientific studies.

To conclude, image-guided online ART allowing for higher dose levels in the target volume, at similar or even reduced dose burden to close-by OARs, is currently entering radiotherapy clinics. Hereby, a considerably more efficient patient treatment is expected, especially in the presence of inter-fractional anatomical changes. The research performed in the scope of this habilitation addressed various aspects of MRI- and CBCT-guided ART with photons and protons paving the way towards clinical adoption of these radiotherapy techniques.

4 List of abbreviations

ART	Adaptive radiotherapy
CBCT	Cone-beam computed tomography
CNN	Convolutional neural network
CT	Computed tomography
DIR	Deformable image registration
DVH	Dose-volume-histogram
DWI	Diffusion-weighted imaging
GAN	Generative adversarial network
H&N	Head and neck
HU	Hounsfield units
ICCP	Iso-center planning problem
IMPT	Intensity-modulated proton therapy
IMRT	Intensity-modulated radiotherapy
ITWM	Fraunhofer Institute for Industrial Mathematics
Linac	Linear accelerator
LMU	Ludwig-Maximilians-University
LUT	Look-up table
MCO	Multi-criteria optimization
MRCAT	MR for calculating attenuation
MRI	Magnetic resonance imaging
OAR	Organ-at-risk
PET	Positron emission tomography
sCT	Synthetic CT
vCT	Virtual CT

5 Literature

1. Acharya S, Fischer-Valuck BW, Kashani R, Parikh P, Yang D, Zhao T, et al. Online Magnetic Resonance Image Guided Adaptive Radiation Therapy: First Clinical Applications. Int J Radiat Oncol Biol Phys. 2016;94(2):394-403.

2. Alaei P, Spezi E. Imaging dose from cone beam computed tomography in radiation therapy. Phys Med. 2015;31(7):647-58.

3. Ardila D, Kiraly AP, Bharadwaj S, Choi B, Reicher JJ, Peng L, et al. End-to-end lung cancer screening with three-dimensional deep learning on low-dose chest computed tomography. Nat Med. 2019;25(6):954-61.

4. Balagopal A, Kazemifar S, Nguyen D, Lin MH, Hannan R, Owrangi A, et al. Fully automated organ segmentation in male pelvic CT images. Phys Med Biol. 2018;63(24):245015.

5. Bert C, Durante M. Motion in radiotherapy: particle therapy. Phys Med Biol. 2011;56(16):R113-44.

6. Bohoudi O, Bruynzeel AME, Senan S, Cuijpers JP, Slotman BJ, Lagerwaard FJ, et al. Fast and robust online adaptive planning in stereotactic MR-guided adaptive radiation therapy (SMART) for pancreatic cancer. Radiother Oncol. 2017;125(3):439-44.

7. Dinkla AM, Wolterink JM, Maspero M, Savenije MHF, Verhoeff JJC, Seravalli E, et al. MR-Only Brain Radiation Therapy: Dosimetric Evaluation of Synthetic CTs Generated by a Dilated Convolutional Neural Network. Int J Radiat Oncol Biol Phys. 2018;102(4):801-12.

8. Draulans C, van der Heide UA, Haustermans K, Pos FJ, van der Voort van Zyp J, De Boer H, et al. Primary endpoint analysis of the multicentre phase II hypo-FLAME trial for intermediate and high risk prostate cancer. Radiother Oncol. 2020;147:92-8.

9. Durante M, Loeffler JS. Charged particles in radiation oncology. Nat Rev Clin Oncol. 2010;7(1):37-43.

10. Edmund JM, Nyholm T. A review of substitute CT generation for MRI-only radiation therapy. Radiat Oncol. 2017;12(1):28.

11. Esteva A, Kuprel B, Novoa RA, Ko J, Swetter SM, Blau HM, et al. Dermatologist-level classification of skin cancer with deep neural networks. Nature. 2017;542(7639):115-8.

12. Fotina I, Hopfgartner J, Stock M, Steininger T, Lutgendorf-Caucig C, Georg D. Feasibility of CBCT-based dose calculation: comparative analysis of HU adjustment techniques. Radiother Oncol. 2012;104(2):249-56.

13. Goodfellow IJ, Pouget-Abadie J, Mirza M, Xu B, Warde-Farley D, Ozair S, et al. Generative Adversarial Networks. arXiv e-prints [Internet]. 2014 June 01, 2014. Available from: https://ui.adsabs.harvard.edu/abs/2014arXiv1406.2661G.

14. Guerreiro F, Koivula L, Seravalli E, Janssens GO, Maduro JH, Brouwer CL, et al. Feasibility of MRI-only photon and proton dose calculations for pediatric patients with abdominal tumors. Phys Med Biol. 2019;64(5):055010.

15. Han X. MR-based synthetic CT generation using a deep convolutional neural network method. Med Phys. 2017;44(4):1408-19.

16. Hansen DC, Landry G, Kamp F, Li M, Belka C, Parodi K, et al. ScatterNet: A convolutional neural network for cone-beam CT intensity correction. Med Phys. 2018;45(11):4916-26.

17. Harms J, Lei Y, Wang T, Zhang R, Zhou J, Tang X, et al. Paired cycle-GAN-based image correction for quantitative cone-beam computed tomography. Med Phys. 2019;46(9):3998-4009.

18. He K, Zhang X, Ren S, Sun J. Deep Residual Learning for Image Recognition2015 December 01, 2015:[arXiv:1512.03385 p.]. Available from: https://ui.adsabs.harvard.edu/abs/2015arXiv151203385H.

19. Ibragimov B, Xing L. Segmentation of organs-at-risks in head and neck CT images using convolutional neural networks. Med Phys. 2017;44(2):547-57.

20. Jaffray DA. Image-guided radiotherapy: from current concept to future perspectives. Nat Rev Clin Oncol. 2012;9(12):688-99.

21. Jelercic S, Rajer M. The role of PET-CT in radiotherapy planning of solid tumours. Radiol Oncol. 2015;49(1):1-9.

22. Jones KM, Michel KA, Bankson JA, Fuller CD, Klopp AH, Venkatesan AM. Emerging Magnetic Resonance Imaging Technologies for Radiation Therapy Planning and Response Assessment. Int J Radiat Oncol Biol Phys. 2018;101(5):1046-56.

23. Kida S, Nakamoto T, Nakano M, Nawa K, Haga A, Kotoku J, et al. Cone Beam Computed Tomography Image Quality Improvement Using a Deep Convolutional Neural Network. Cureus. 2018;10(4):e2548.

24. Knopf AC, Lomax A. In vivo proton range verification: a review. Phys Med Biol. 2013;58(15):R131-60.

25. Koivula L, Wee L, Korhonen J. Feasibility of MRI-only treatment planning for proton therapy in brain and prostate cancers: Dose calculation accuracy in substitute CT images. Med Phys. 2016;43(8):4634.

26. Korreman SS. Motion in radiotherapy: photon therapy. Phys Med Biol. 2012;57(23):R161-91.

27. Kurz C, Dedes G, Resch A, Reiner M, Ganswindt U, Nijhuis R, et al. Comparing cone-beam CT intensity correction methods for dose recalculation in adaptive intensity-modulated photon and proton therapy for head and neck cancer. Acta Oncol. 2015;54(9):1651-7.

28. Lagendijk JJ, Raaymakers BW, Van den Berg CA, Moerland MA, Philippens ME, van Vulpen M. MR guidance in radiotherapy. Phys Med Biol. 2014;59(21):R349-69.

29. Lagendijk JJ, Raaymakers BW, van Vulpen M. The magnetic resonance imaging-linac system. Semin Radiat Oncol. 2014;24(3):207-9.

30. Landry G, Nijhuis R, Dedes G, Handrack J, Thieke C, Janssens G, et al. Investigating CT to CBCT image registration for head and neck proton therapy as a tool for daily dose recalculation. Med Phys. 2015;42(3):1354-66.

31. Liu Y, Lei Y, Wang Y, Wang T, Ren L, Lin L, et al. MRI-based treatment planning for proton radiotherapy: dosimetric validation of a deep learning-based liver synthetic CT generation method. Phys Med Biol. 2019;64(14):145015.

32. Maier J, Eulig E, Voth T, Knaup M, Kuntz J, Sawall S, et al. Real-time scatter estimation for medical CT using the deep scatter estimation: Method and robustness analysis with respect to different anatomies, dose levels, tube voltages, and data truncation. Med Phys. 2019;46(1):238-49.

33. Maspero M, Savenije MHF, Dinkla AM, Seevinck PR, Intven MPW, Jurgenliemk-Schulz IM, et al. Dose evaluation of fast synthetic-CT generation using a generative adversarial network for general pelvis MR-only radiotherapy. Phys Med Biol. 2018;63(18):185001.

34. Maspero M, van den Berg CAT, Landry G, Belka C, Parodi K, Seevinck PR, et al. Feasibility of MR-only proton dose calculations for prostate cancer radiotherapy using a commercial pseudo-CT generation method. Phys Med Biol. 2017;62(24):9159-76.

35. Milletari F, Navab N, Ahmadi S-A. V-Net: Fully Convolutional Neural Networks for Volumetric Medical Image Segmentation. arXiv e-prints [Internet]. 2016 June 01, 2016. Available from: https://ui.adsabs.harvard.edu/abs/2016arXiv160604797M.

36. Mutic S, Dempsey JF. The ViewRay system: magnetic resonance-guided and controlled radiotherapy. Semin Radiat Oncol. 2014;24(3):196-9.

37. Neppl S, Landry G, Kurz C, Hansen DC, Hoyle B, Stöcklein S, et al. Evaluation of proton and photon dose distributions recalculated on 2D and 3D Unet-generated pseudoCTs from T1-weighted MR head scans. Acta Oncol. 2019:1-6.

38. Nie D, Wang L, Gao Y, Lian J, Shen D. STRAINet: Spatially Varying sTochastic Residual AdversarIal Networks for MRI Pelvic Organ Segmentation. IEEE Trans Neural Netw Learn Syst. 2019;30(5):1552-64.

39. Niu T, Al-Basheer A, Zhu L. Quantitative cone-beam CT imaging in radiation therapy using planning CT as a prior: first patient studies. Med Phys. 2012;39(4):1991-2000.

40. Oborn BM, Dowdell S, Metcalfe PE, Crozier S, Mohan R, Keall PJ. Future of medical physics: Real-time MRI-guided proton therapy. Med Phys. 2017;44(8):e77-e90.

41. Park YK, Sharp GC, Phillips J, Winey BA. Proton dose calculation on scatter-corrected CBCT image: Feasibility study for adaptive proton therapy. Med Phys. 2015;42(8):4449-59.

42. Pileggi G, Speier C, Sharp GC, Izquierdo Garcia D, Catana C, Pursley J, et al. Proton range shift analysis on brain pseudo-CT generated from T1 and T2 MR. Acta Oncol. 2018;57(11):1521-31.

43. Raaymakers BW, Jurgenliemk-Schulz IM, Bol GH, Glitzner M, Kotte A, van Asselen B, et al. First patients treated with a 1.5 T MRI-Linac: clinical proof of concept of a high-precision, high-field MRI guided radiotherapy treatment. Phys Med Biol. 2017;62(23):L41-L50.

44. Robert Koch-Institut. Krebs in Deutschland für 2013/2014: Gesellschaft der epidemiologischen Krebsregister e.V. (GEKID) und Zentrum für Krebsregisterdaten (ZfKD); 2017.

45. Ronneberger O, Fischer P, Brox T, editors. U-Net: Convolutional Networks for Biomedical Image Segmentation. MICCAI; 2015.

46. Rudra S, Jiang N, Rosenberg SA, Olsen JR, Roach MC, Wan L, et al. Using adaptive magnetic resonance image-guided radiation therapy for treatment of inoperable pancreatic cancer. Cancer Med. 2019;8(5):2123-32.

47. Schellhammer SM, Hoffmann AL, Gantz S, Smeets J, van der Kraaij E, Quets S, et al. Integrating a low-field open MR scanner with a static proton research beam line: proof of concept. Phys Med Biol. 2018;63(23):23LT01.

48. Schmidt MA, Payne GS. Radiotherapy planning using MRI. Phys Med Biol. 2015;60(22):R323-61.

49. Spadea MF, Pileggi G, Zaffino P, Salome P, Catana C, Izquierdo-Garcia D, et al. Deep Convolution Neural Network (DCNN) Multiplane Approach to Synthetic CT Generation From MR images-Application in Brain Proton Therapy. Int J Radiat Oncol Biol Phys. 2019;105(3):495-503.

50. van Herk M. Errors and margins in radiotherapy. Semin Radiat Oncol. 2004;14(1):52-64.

51. van Sornsen de Koste JR, Palacios MA, Bruynzeel AME, Slotman BJ, Senan S, Lagerwaard FJ. MR-guided Gated Stereotactic Radiation Therapy Delivery for Lung, Adrenal, and Pancreatic Tumors: A Geometric Analysis. Int J Radiat Oncol Biol Phys. 2018;102(4):858-66.

52. Webb S. The physical basis of IMRT and inverse planning. Br J Radiol. 2003;76(910):678-89.

53. Werensteijn-Honingh AM, Kroon PS, Winkel D, Aalbers EM, van Asselen B, Bol GH, et al. Feasibility of stereotactic radiotherapy using a 1.5T MR-linac: Multi-fraction treatment of pelvic lymph node oligometastases. Radiother Oncol. 2019;134:50-4.

54. Yan D, Vicini F, Wong J, Martinez A. Adaptive radiation therapy. Phys Med Biol. 1997;42(1):123-32.

6 Acknowledgements

At first, I would like to thank Prof. Claus Belka for the opportunity to pursue my habilitation at the LMU Department of Radiation Oncology under his supervision. I want to thank Prof. Katia Parodi and Prof. Peter Bartenstein for taking over the duties in the Fachmentorat.

The research projects leading up to this habilitation were performed over the past six years at the LMU Department of Medical Physics, the Department of Radiotherapy at UMC Utrecht and the LMU Department of Radiation Oncology. Thus, I would like to acknowledge the continuous support by the respective heads of departments: Prof. Katia Parodi, Prof. Bas Raaymakers and Prof. Claus Belka.

This work would also not have been possible without the help of many colleagues, who were also majorly responsible for making daily research work so cheerful. Not everybody who has contributed can be mentioned here. Nevertheless, I want to take the chance to thank Florian Kamp, Moritz Rabe, Sebastian Neppl, Jan Hofmaier, Christian Thieke and Michael Reiner from the LMU Department of Radiation Onocology, as well as George Dedes, Marco Pinto and Marco Riboldi from the LMU Department of Medical Physics. At UMC Utrecht, I would like to gratefully acknowledge the support by Matteo Maspero, Mark Savenije and Nico van den Berg. A special thank goes to Guillaume Landry for his substantial contributions and the close collaboration in the scope of this habilitation project.

I also want to thank the external collaborators that gave crucial input for my work: Philipp Süss, Jonas Haehnle and Katrin Teichert from ITWM Kaiserslautern, Simon Rit from CREATIS Lyon, Guillaume Janssens from IBA, Yang Kyun Park (formerly) from MGH Boston, as well as David Hansen (formerly) from the Aarhus University Hospital.

Last, but certainly not least, I would like to thank my friends and my family, especially my parents and my sister, for their continuous support.

7 Declaration

Hiermit versichere ich an Eides statt, dass ich meine Habilitationsleistung selbständig und ohne andere als die angegebenen Hilfsmittel angefertigt habe, zudem die Herkunft des verwendeten und zitierten Materials ordnungsgemäß kenntlich gemacht habe.

Des Weiteren erkläre ich, dass ich mich weder anderweitig habilitiert, noch bereits Habilitationsversuche unternommen habe und dass mir kein akademischer Grad entzogen wurde oder ein Verfahren gegen mich anhängig ist, welches zur Entziehung eines akademischen Grades führen könnte.

München, 26. August 2020

Dr. rer. nat. Christopher Kurz

8 Facsimile of relevant scientific contributions

Only contributions not infringing any copyrights will be included in the following. All further contributions, including all relevant information, can be found on page 1 of this thesis.

Acta Oncologica, 2015; 54: 1651–1657

Taylor & Francis
Taylor & Francis Group

ORIGINAL ARTICLE

Comparing cone-beam CT intensity correction methods for dose recalculation in adaptive intensity-modulated photon and proton therapy for head and neck cancer

CHRISTOPHER KURZ[1,2], GEORGE DEDES[2], ANDREAS RESCH[2], MICHAEL REINER[1], UTE GANSWINDT[1], REINOUD NIJHUIS[1], CHRISTIAN THIEKE[1], CLAUS BELKA[1], KATIA PARODI[2] & GUILLAUME LANDRY[1,2]

[1]*Department of Radiation Oncology, Ludwig-Maximilians-University, Munich, Germany and* [2]*Department of Medical Physics, Ludwig-Maximilians-University, Munich, Germany*

ABSTRACT

Background. Adaptive intensity-modulated photon and proton radiotherapy (IMRT and IMPT) of head and neck (H&N) cancer requires frequent three-dimensional (3D) dose calculation. We compared two approaches for dose recalculation on the basis of intensity-corrected cone-beam (CB) x-ray computed tomography (CT) images.

Material and methods. For nine H&N tumor patients, virtual CTs (vCT) were generated by deformable image registration of the planning CT (pCT) to the CBCT. The second intensity correction approach used population-based lookup tables for scaling CBCT intensities to the pCT HU range ($CBCT_{LUT}$). IMRT and IMPT plans were generated with a commercial treatment planning system. Dose recalculations on vCT and $CBCT_{LUT}$ were analyzed using a (3%, 3 mm) gamma-index analysis and comparison of normal tissue and tumor dose/volume parameters. A replanning CT (rpCT) acquired within three days of the CBCT served as reference. Single field uniform dose (SFUD) proton plans were created and recalculated on vCT and $CBCT_{LUT}$ for proton range comparison.

Results. Dose/volume parameters showed minor differences between rpCT, vCT and $CBCT_{LUT}$ in IMRT, but clinically relevant deviations between $CBCT_{LUT}$ and rpCT in the spinal cord for IMPT. Gamma-index pass-rates were found increased for vCT with respect to $CBCT_{LUT}$ in IMPT (by up to 21 percentage points) and IMRT (by up to 9 percentage points) for most cases. The SFUD-based proton range assessment showed improved agreement of vCT and rpCT, with 88–99% of the depth dose profiles in beam's eye view agreeing within 3 mm. For $CBCT_{LUT}$, only 80–94% of the profiles fulfilled this criterion.

Conclusion. vCT and $CBCT_{LUT}$ are suitable options for dose recalculation in adaptive IMRT. In the scope of IMPT, the vCT approach is preferable.

During the course of fractionated radiotherapy of head and neck (H&N) cancer, considerable anatomical changes may occur [1] and substantially compromise treatment quality. An adaptation of the planned treatment might, therefore, be necessary [2]. For deciding if and how to adapt, a three-dimensional (3D) dose calculation on the anatomy at the time of adaptation is required.

In photon intensity-modulated radiation therapy (IMRT), the widespread use of repeated cone-beam x-ray computed tomography (CBCT) imaging [3] for patient positioning yields data sets which can also be used to evaluate the daily 3D IMRT dose distribution [4]. This was investigated by several groups using varying degrees of refinement in the conversion of CBCT numbers to electron density [5–13]. Approaches range from using calibration curves (phantom or patient data based) to the application of deformable image registration (DIR). Recently, also intensity-modulated proton therapy (IMPT) has been applied to the treatment of H&N lesions [14,15]. First comparisons of IMPT and IMRT in adaptive treatment scenarios have been published [16,17] and IMPT clinics are beginning to adopt IMRT-inspired CBCT-based image

Correspondence: C. Kurz, Am Coulombwall 1, 85748 Garching, Germany. Tel: +49 89 289 14022. E-mail: christopher.kurz@physik.uni-muenchen.de

(Received 16 May 2015; accepted 8 June 2015)

ISSN 0284-186X print/ISSN 1651-226X online © 2015 Informa Healthcare
DOI: 10.3109/0284186X.2015.1061206

guidance. This opens the door to IMRT-like strategies for treatment adaptation on the basis of dose recalculations. CBCT intensity correction by deforming the planning CT to the CBCT has been shown to enable IMPT dose recalculation to an acceptable level of accuracy on the basis of clinical CBCT images [18]. However, DIR-based methods are relatively complicated and require careful evaluation. To the best of our knowledge there is no evidence in the literature that a simpler intensity correction method is inadequate for IMPT dose recalculation of H&N cases.

This work aims at comparing the DIR-based intensity correction approach to a simpler CBCT to CT intensity rescaling method with population-based calibration curves for dose recalculation in IMPT and IMRT for H&N cancer. For both, IMPT and IMRT, recalculated dose distributions on intensity-corrected CBCT images and a reference replanning CT acquired close in time were compared using dose/volume parameters and gamma-index evaluation. For IMPT, where the concept of range is critical, single field uniform dose (SFUD) distributions were also compared in terms of proton range.

Material and methods

Clinical data

Dose and imaging data from nine patients previously treated with IMRT for H&N cancer, of which six patients had caudally (PCA1–6) and three cranially (PCR1–3) located tumors, were used in this study. For each subject, a planning CT (pCT), a replanning CT (rpCT), and a CBCT was available. The pCT and rpCT included all relevant tumor and normal tissue structures that had been manually delineated by the same physician (high and low dose clinical and planning target volumes (CTV, PTV), parotids, brain stem, spinal cord, chiasm, optical nerves, eyes and eye lenses). CBCT and rpCT were acquired at most three days apart (population median: one day), with the rpCT being taken between 33 and 51 days after the pCT. Details on the patient cases can be found in Supplementary Table I (available online at http://informahealthcare.com/doi/abs/10.3109/0284186X.2015.1061206), including also the target dose prescriptions. pCT and rpCT images (acquired with a Toshiba Aquilion LB scanner) were reconstructed on a 1.074 mm $\times$ 1.074 mm $\times$ 3 mm grid, CBCT images (acquired with the on-board Elekta Synergy Linac imager equipped with XVI R4.5) on a 1 mm $\times$ 1 mm $\times$ 1 mm grid.

CBCT intensity correction

The first CBCT intensity correction approach is based on DIR of the pCT to the CBCT, yielding a so-called virtual CT (vCT). A Morphons algorithm [19,20] has been used following the approach described and validated in [18,21] with only slight modifications: the initial alignment of the CBCT and pCT not only included a translational registration but also allowed for rotations, mimicking patient positioning with a modern 6-degrees-of-freedom table. This rigid registration was performed on a region of interest (ROI) containing the spine from the first to the sixth vertebrae for PatCA1–6 and the skull for PatCR1–3. Regions outside the CBCT field-of-view (FOV) were stitched with the corresponding pCT data in order to simulate a clinical adaptation scenario where a rpCT is not available.

The second intensity correction approach uses a population-based CBCT intensity rescaling. The CBCT image was aligned to the pCT applying the same rigid registration as during the vCT generation. Regions outside the CBCT FOV were again stitched with the pCT data. CT numbers were sampled at various points from both, the original pCT and the aligned CBCT, in the air outside the patient, the air inside the airways, fatty tissue, muscle, brain tissue (only PatCR1–3), soft and hard bone. These data were used to generate a CBCT to pCT Hounsfield number lookup table (HLUT) that was applied for CBCT intensity correction, yielding a so-called $CBCT_{LUT}$. Due to varying CBCT intensities within the FOV, it was found necessary to establish separate HLUTs for patients with caudally and cranially located lesions by sampling HLUT points in muscle, fat and bony structures either in the neck (PatCA1–6) or the skull-base region (PatCR1–3). The applied HLUTs are shown in Supplementary Figure 1 (available online at http://informahealthcare.com/doi/abs/10.3109/0284186X.2015.1061206).

Registration: rpCT

To enable dose recalculation on the rpCT images, considered as reference in our study, they were aligned to the corresponding pCT by a rigid registration including translation and rotation, focusing on similar ROIs as used in the pCT to CBCT registration. Manual tuning of the final rigid registrations yielded corrections smaller than 1 mm.

Treatment planning and data evaluation

A research version of a commercial treatment planning system (TPS) (RayStation 4.6, RaySearch Laboratories, Stockholm, Sweden) was used to generate IMRT and IMPT plans for each patient on the basis of the pCT. The original clinical IMRT plans were used as templates and we aimed at reproducing equivalent dose distributions in terms of dose/

volume parameters. The organ at risk (OAR) dose/volume constraints used for treatment planning are summarized in Supplementary Table II (available online at http://informahealthcare.com/doi/abs/10.3109/0284186X.2015.1061206). The clinical IMRT plans consisted of a simultaneous integrated boost (SIB) with two dose levels (see Supplementary Table I available online at http://informahealthcare.com/doi/abs/10.3109/0284186X.2015.1061206) in 25–32 fractions, followed by a sequential boost with five 2 Gy fractions. The boost phase was not considered in this work. Between nine (for caudal H&N lesions) and 11 (for cranial lesions) beam angles have been used in IMRT. The IMPT plans used a four-field arrangement for the caudal cases (45°, 90°, 270° and 315°; 90° and 270° blocked in shoulder area), and a three-field arrangement for the cranial cases (0°, 100° and 260°; 0° blocked in nasal/buccal cavity). A constant proton RBE (relative biological effectiveness) of 1.1 was considered throughout the study and results will be given in terms of RBE-weighted dose. For probing the proton range, SFUD plans have additionally been generated on the rpCT using a single gantry angle (see Supplementary Table I available online at http://informahealthcare.com/doi/abs/10.3109/0284186X.2015.1061206) and aiming at covering the high dose PTV. By using the rpCT for SFUD optimization, dose distributions with sharp gradients on the considered CT images could be obtained. For the SFUD plans, a dose grid with 1 mm instead of 3 mm axial spacing was employed to yield higher resolution range probing.

For dosimetric comparison of the CBCT intensity correction approaches, IMRT and IMPT plans were recalculated on the rpCT, vCT and $CBCT_{LUT}$ images using built-in TPS functionalities. The contours from the rpCT were copied to the aligned vCT and $CBCT_{LUT}$ images for dose/volume parameter evaluation. Due to the low elapsed time between rpCT and CBCT acquisitions, no contour correction was required except for the patient outline, which was updated on the vCT and copied to the $CBCT_{LUT}$ due to differences in the shoulder region by stitching the pCT. We recorded high and low dose PTV D_{95} and V_{95}, spinal cord and brain stem D_2, as well as parotid D_{mean} for all recalculated dose distributions. For PatCR1-3, the optical nerve, chiasm and eye D_2, as well as the eye lens D_{mean} were additionally considered. The vCT and $CBCT_{LUT}$ dose distributions were also compared to the reference rpCT dose distribution by means of a 3D global gamma-index analysis using (3%, 3 mm) criteria and considering voxels with a single fraction dose above 1 Gy.

For proton range evaluation, the rpCT-based SFUD plans have been recalculated on the vCT as well as the $CBCT_{LUT}$ and the proton ranges, defined as distances from the patient surface to the 80% dose fall-off in beam's eye view (BEV), have been compared to that of the rpCT dose distribution.

Results

Registration

Compared to the reference rpCT, a good agreement of bony structures, internal air cavities and outer contour was observed for the vCT and the $CBCT_{LUT}$. Differences between the two intensity correction methods arise close to the skull base and, in particular, between the shoulders of the patients. Here, the CBCT image is affected by severe artifacts and shadowing (see Supplementary Figure 2, available online at http://informahealthcare.com/doi/abs/10.3109/0284186X.2015.1061206). This cannot be recovered by the applied CT number rescaling, which was found to be only accurate in the spatially restricted region where the population-based CT to CBCT HLUT has been retrieved.

Dose distribution comparison

The dose distributions from IMRT and IMPT were found comparable on rpCT, vCT and $CBCT_{LUT}$ in regions where the CBCT is less affected by artifacts and the used HLUT-based rescaling accurate (see Figure 1, top rows). In the region between the shoulders, however, the formation of hotspots in the IMRT recalculation and a severe distortion of the IMPT dose pattern are observed (see Figure 1, bottom rows). The proton ranges are not correctly preserved, resulting in a considerably increased dose to the spinal cord for patients with an anteriorly positioned PTV (see Supplementary Figure 3, available online at http://informahealthcare.com/doi/abs/10.3109/0284186X.2015.1061206).

The dose/volume parameters of the recalculated 3D IMRT dose distributions were found close to the rpCT values for vCT and $CBCT_{LUT}$, as illustrated in Figure 2. Most parameters were found to agree within 1 Gy (considering the total dose of the SIB treatment phase), indicating no clinically relevant differences between the two intensity correction approaches in this respect. In IMPT, larger differences of the dose/volume parameters with respect to the rpCT were found for both intensity correction techniques (see Figure 2). Typically, deviations are below 4 Gy and similar for vCT and $CBCT_{LUT}$, except for the spinal cord where differences up to 20 Gy emerge for the $CBCT_{LUT}$.

In terms of the gamma-index analysis, slightly enhanced pass-rates for the vCT with respect to the $CBCT_{LUT}$ were observed for the caudal H&N cases (91–97% against 85–93%) in IMRT (Table I). For

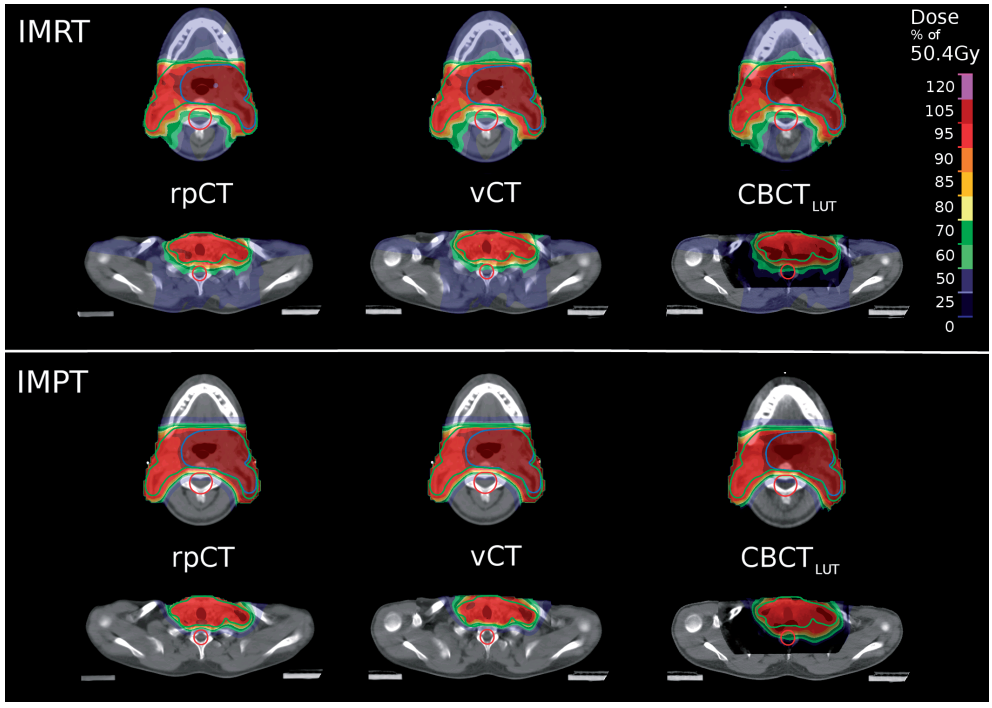

Figure 1. 2D IMRT (top part) and IMPT (bottom part) dose distributions (color-wash) on the investigated CT datasets for PatCA6 in an upper (top row of each part) and lower (bottom row) axial slice. The low and high dose PTVs (green and blue structures), as well as the spinal cord planning organ at risk volume (PRV, red structure) are also shown.

the cranial cases, an equal performance was found. In IMPT, gamma-index pass-rates were overall smaller with respect to IMRT, particularly for the caudal H&N cases due to more pronounced deviations in the patients shoulder region (cf. Supplementary Figure 4, available online at http://informahealthcare.com/doi/abs/10.3109/0284186X.2015.1061206). Differences between vCT and $CBCT_{LUT}$ pass-rates (76–95% against 74–88%) were larger than in IMRT. For the cranial cases, however, comparable performances of both intensity correction strategies were identified and pass-rates similar to IMRT obtained.

Proton range comparison

The amount of 1D profiles exhibiting a range deviation of less than 3 mm with respect to the rpCT was found increased for the vCT (89–95%) with respect to the $CBCT_{LUT}$ recalculations (80–94%, see Table I). Differences between both approaches were mainly located close to the skull base and in the shoulder region, were the CBCT intensities are typically reduced due to artifacts. For patients where the high dose PTV was located in regions with reduced artifacts in the CBCT and comparably stable CT numbers (PatCA2–4, see Supplementary Table IV, available online at http://informahealthcare.com/doi/abs/10.3109/0284186X.2015.1061206), only minor differences between vCT and $CBCT_{LUT}$ were identified.

Discussion

In this work, a DIR-based CBCT intensity correction approach (vCT) has been compared to a population-based calibration approach ($CBCT_{LUT}$) in the context of dose recalculation for adaptive IMRT and IMPT for the first time. The results indicate a comparable performance of both intensity correction techniques in the scope of IMRT. However, although differences in the investigated dose/volume parameters with respect to the rpCT were mostly below 1 Gy, the gamma-index analysis, being more sensitive to local dose changes, pointed out slight inaccuracies in the $CBCT_{LUT}$ recalculation in the shoulder region. Here, the severe shadowing in the CBCT is not recovered by the applied intensity rescaling and the DIR-based approach yields improved agreement to the rpCT dose distribution as it adapts the pCT with its correct CT numbers to the CBCT anatomy. For the cranial cases, the PTV does not extend to this area and very similar gamma-index pass-rates for $CBCT_{LUT}$ and vCT were found.

Due to the steeper dose gradients, the finite particle range and the reduced number of applied beams, differences between vCT and $CBCT_{LUT}$, and between these two approaches and the reference rpCT are larger in IMPT. While vCT and $CBCT_{LUT}$ provide comparable results for the cranial H&N cases, a notable benefit by using the vCT was found for the caudal H&N cases. In the dose/volume parameter analysis,

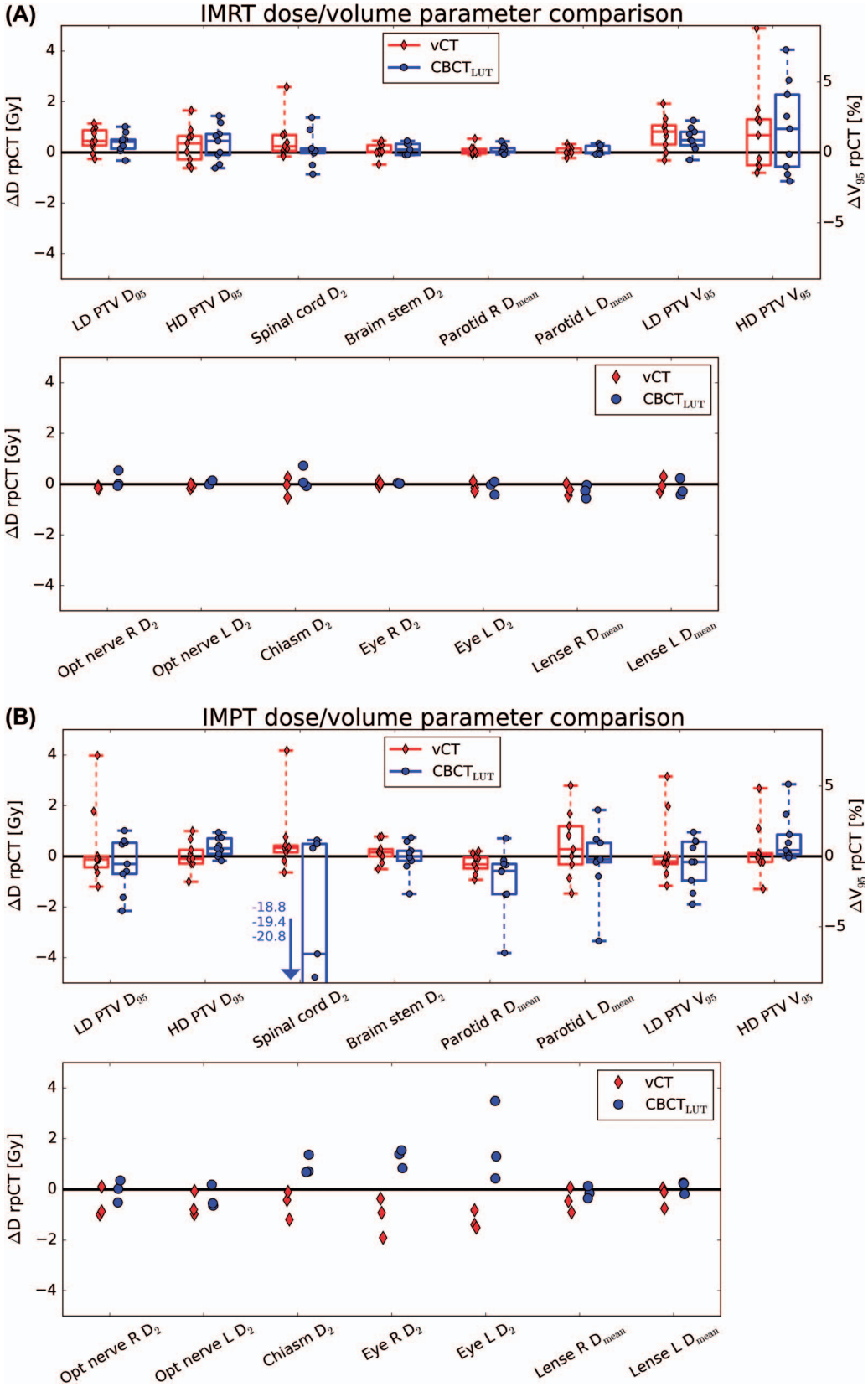

Figure 2. Comparison of IMRT (A, top) and IMPT (B, bottom) dose/volume parameters for vCT (red, diamonds) and $CBCT_{LUT}$ (blue, circles) dose recalculations. The dosimetric parameters correspond to the left, V_{95} to the right axis. For each parameter, the difference to the rpCT reference is given for every patient considering the total dose of the SIB treatment phase. For the optical system (only three patients) no boxplots were generated. For display purposes, data points below -5Gy difference are indicated by the arrow but not shown.

Table I. Gamma-index and proton range pass-rates for vCT and $CBCT_{LUT}$ dose recalculations.

	Gamma-index pass-rates				BEV range pass-rates	
	IMRT		IMPT		IMPT	
	vCT (%)	$CBCT_{LUT}$ (%)	vCT (%)	$CBCT_{LUT}$ (%)	vCT (%)	$CBCT_{LUT}$ (%)
PatCA1–6	95 (91,97)	89 (85,93)	90 (76,95)	80 (74,88)	93 (88,95)	87 (80,94)
PatCR1–3	96 (89,99)	97 (92,99)	95 (93,98)	95 (90,97)	95 (89,99)	85 (80,88)

The vCT- and $CBCT_{LUT}$-based dose recalculation is compared to the rpCT-based recalculation for the patients with caudal (PatCA1–6) and cranial (PatCR1-3) lesions. Pass rates of the (3%, 3 mm) gamma evaluation are shown for IMRT and IMPT, together with the amount of 1D BEV proton dose profiles exhibiting a range within 3 mm of the rpCT SFUD distribution. The mean value over the considered patients and the minimum/maximum pass-rates (in brackets) are reported. Individual patient values can be found in Supplementary Tables III and IV in the appendix.

this was particularly indicated by an improved agreement of the vCT and rpCT spinal cord D_2 which could be overestimated to a clinically unacceptable level of up to 20 Gy in the $CBCT_{LUT}$ recalculation. Moreover, the vCT shows enhanced gamma-index pass-rates and improved range agreement, as assessed by the recalculated SFUD proton dose distributions. Even for the cranially located lesions, where very similar gamma-index pass-rates for vCT and $CBCT_{LUT}$ were found, an improved range agreement to the reference was identified for the vCT. The results suggest decreased differences between the investigated CBCT correction approaches for multiple field proton plans, where range deviations are less critical due to overlapping beams from different angles. It should also be mentioned that no correlation between the time elapsed between CBCT and rpCT imaging and the gamma-index pass-rate was found. This is probably due to the fact that anatomical deviations are mainly attributed to positioning uncertainties rather than internal anatomical changes which typically evolve on longer time-scales.

The identified shortcomings of the $CBCT_{LUT}$ approach are strongly related to intrinsic CBCT artifacts, in particular shadowing effects that cannot be corrected for by the HLUT-based intensity rescaling. Dose recalculation accuracy also suffers from variation of CT numbers within the FOV, such that the $CBCT_{LUT}$ can only be accurate in a restricted part of the FOV, often being smaller than the extended target volumes of H&N cancer patients. Separate HLUT scaling tables for different locations of the high dose PTVs are thus deemed necessary. Eventually, major improvements of CBCT intensity rescaling approaches can only be expected from more advanced CBCT instrumentation (e.g. with larger FOV), improved reconstruction techniques with reduced artifacts and more accurate image intensities [22,23] or potentially by application of compressed sensing approaches. Although the $CBCT_{LUT}$ approach is computationally inexpensive, it has to be noted that initial generation of the used HLUT table is a time consuming manual procedure. In future, this procedure could, however, be automated by applying techniques like scale-invariant feature transform [24] to identify matching points in the CBCT and pCT and retrieve the corresponding CT numbers for input to the HLUT. DIR-based CBCT correction approaches, on the other hand, require thorough initial quality control of the applied registration algorithm and of the obtained deformation fields.

Beyond the previously discussed advantages, the DIR approach enables automatic generation of up-to-date structures on the generated vCT by warping the contours delineated on the pCT to the recent patient anatomy of the CBCT [18]. This is a substantial advantage over the CBCT intensity rescaling approach since segmentation on the low-contrast, artifact-prone CBCT images is a challenging, highly time consuming task and since an up-to-date delineation is an indispensable prerequisite for adaptive radiotherapy.

In summary, we have carefully compared DIR- and lookup table-based CBCT intensity correction techniques for IMRT and IMPT of H&N cancers. In IMPT, thorough investigation of the proton range was included in addition to DVH and gamma-index analysis. The DIR-based CBCT correction is deemed a suitable tool to foster adaptive IMRT and IMPT by providing accurate and up-to-date 3D dose recalculations and structures. The simpler population-based scaling approach is considered sufficiently accurate in the context of IMRT, but shows considerable shortcomings in IMPT.

Acknowledgements

This work was supported by the Federal Ministry of Education and Research of Germany (BMBF), Grant No. 01IB13001 (SPARTA), and by the German Research Foundation (DFG) Cluster of Excellence Munich-Centre for Advanced Photonics (MAP). The authors thank Guillaume Janssens and Jonathan Orban de Xivry for sharing the REGGUI toolkit containing the implementation of the

Morphons algorithm. Helpful advice concerning IMPT treatment planning from Silvia Molinelli, Mario Ciocca, Martin Hillbrand, Daniel Koepl, Franz Joachim Kaizer and Barbara Knäusl is gratefully acknowledged. We thank Erik Traneus from RaySearch Laboratories for his support on the RayStation TPS.

Declaration of interest: The authors report no conflicts of interest. The authors alone are responsible for the content and writing of the paper.

References

[1] Barker JL, Garden AS, Ang KK, O'Daniel JC, Wang H, Court LE, et al. Quantification of volumetric and geometric changes occurring during fractionated radiotherapy for head-and-neck cancer using an integrated CT/linear accelerator system. Int J Radiat Oncol Biol Phys 2004;59:960–70.

[2] Jensen AD, Nill S, Huber PE, Bendl R, Debus J, Munter MW. A clinical concept for interfractional adaptive radiation therapy in the treatment of head and neck cancer. Int J Radiat Oncol Biol Phys 2012;82:590–6.

[3] Verellen D, De Ridder M, Tournel K, Duchateau M, Reynders T, Gevaert T, et al. An overview of volumetric imaging technologies and their quality assurance for IGRT. Acta Oncol 2008;47:1271–8.

[4] Yang Y, Schreibmann E, Li T, Wang C, Xing L. Evaluation of on-board kV cone beam CT (CBCT)-based dose calculation. Phys Med Biol 2007;52:685–705.

[5] Zhang T, Chi Y, Meldolesi E, Yan D. Automatic delineation of on-line head-and-neck computed tomography images: Toward on-line adaptive radiotherapy. Int J Radiat Oncol Biol Phys 2007;68:522–30.

[6] Wu Q, Chi Y, Chen PY, Krauss DJ, Yan D, Martinez A. Adaptive replanning strategies accounting for shrinkage in head and neck IMRT. Int J Radiat Oncol Biol Phys 2009;75:924–32.

[7] Elstrom UV, Wysocka BA, Muren LP, Petersen JB, Grau C. Daily kV cone-beam CT and deformable image registration as a method for studying dosimetric consequences of anatomic changes in adaptive IMRT of head and neck cancer. Acta Oncol 2010;49:1101–8.

[8] Fotina I, Hopfgartner J, Stock M, Steininger T, Lutgendorf-Caucig C, Georg D. Feasibility of CBCT-based dose calculation: Comparative analysis of HU adjustment techniques. Radiother Oncol 2012;104:249–56.

[9] Peroni M, Ciardo D, Spadea MF, Riboldi M, Comi S, Alterio D, et al. Automatic segmentation and online virtual CT in head-and-neck adaptive radiation therapy. Int J Radiat Oncol Biol Phys 2012;84:e427–33.

[10] Zhen X, Yan H, Zhou L, Jia X, Jiang SB. Deformable image registration of CT and truncated cone-beam CT for adaptive radiation therapy. Phys Med Biol 2013;58:7979–93.

Supplementary material available online

Supplementary Figures 1–4 and Tables I–IV available online at http://informahealthcare.com/doi/abs/10.3109/0284186X.2015.1061206.

[11] Elstrom UV, Olsen SR, Muren LP, Petersen JB, Grau C. The impact of CBCT reconstruction and calibration for radiotherapy planning in the head and neck region – a phantom study. Acta Oncol 2014;53:1114–24.

[12] Veiga C, McClelland J, Moinuddin S, Lourenco A, Ricketts K, Annkah J, et al. Toward adaptive radiotherapy for head and neck patients: Feasibility study on using CT-to-CBCT deformable registration for "dose of the day" calculations. Med Phys 2014;41:031703–1–12.

[13] Moteabbed M, Sharp GC, Wang Y, Trofimov A, Efstathiou JA, Lu HM. Validation of a deformable image registration technique for cone beam CT-based dose verification. Med Phys 2015;42:196–205.

[14] Frank SJ, Cox JD, Gillin M, Mohan R, Garden AS, Rosenthal DI, et al. Multifield optimization intensity modulated proton therapy for head and neck tumors: A translation to practice. Int J Radiat Oncol Biol Phys 2014;89:846–53.

[15] Mendenhall NP, Malyapa RS, Su Z, Yeung D, Mendenhall WM, Li Z. Proton therapy for head and neck cancer: Rationale, potential indications, practical considerations, and current clinical evidence. Acta Oncol 2011;50:763–71.

[16] Simone CB, 2nd, Ly D, Dan TD, Ondos J, Ning H, Belard A, et al. Comparison of intensity-modulated radiotherapy, adaptive radiotherapy, proton radiotherapy, and adaptive proton radiotherapy for treatment of locally advanced head and neck cancer. Radiother Oncol 2011;101:376–82.

[17] Gora J, Kuess P, Stock M, Andrzejewski P, Knäusl B, Paskeviciute B, et al. ART for head and neck patients: On the difference between VMAT and IMPT. Acta Oncol Epub 2015 Apr 8:1–9.

[18] Landry G, Nijhuis R, Dedes G, Handrack J, Thieke C, Janssens G, et al. Investigating CT to CBCT image registration for head and neck proton therapy as a tool for daily dose recalculation. Med Phys 2015;42:1354–66.

[19] Janssens G, Jacques L, Xivry JOd, Geets X, Macq B. Diffeomorphic registration of images with variable contrast enhancement. Int J Biomed Imaging 2011;2011:1–12.

[20] Knutsson H, Andersson M. Morphons: Paint on priors and elastic canvas for segmentation and registration. In: Kalviainen H, Parkkinen J, Kaarna A, editors. Image analysis. Berlin Heidelberg: Springer; 2005. p 292–301.

[21] Landry G, George D, Christoph Zl, Josefine H, Guillaume J, Jonathan Orban de X, et al. Phantom based evaluation of CT to CBCT image registration for proton therapy dose recalculation. Phys Med Biol 2015;60:595–613.

[22] Brock RS, Docef A, Murphy MJ. Reconstruction of a cone-beam CT image via forward iterative projection matching. Med Phys 2010;37:6212–20.

[23] Elstrom UV, Muren LP, Petersen JB, Grau C. Evaluation of image quality for different kV cone-beam CT acquisition and reconstruction methods in the head and neck region. Acta Oncol 2011;50:908–17.

[24] Paganelli C, Peroni M, Riboldi M, Sharp GC, Ciardo D, Alterio D, et al. Scale invariant feature transform in adaptive radiation therapy: A tool for deformable image registration assessment and re-planning indication. Phys Med Biol 2013;58:287–99.

Supplementary material for Kurz et al., Comparing cone-beam CT intensity correction methods for dose recalculation in adaptive intensity modulated photon and proton therapy for head and neck cancer, Acta Oncol, 2015; 54: 1651–1657.

Supplementary Table I. Overview of the investigated patient cohort.

Patient ID	Tumor site	TNM stage	$\Delta t_{rpCT\text{-}CBCT}$ (days)	Prescription low/high dose PTV (Gy)	Number of fractions	SFUD gantry angle (degree)
PatCA1	Larynx	pT2pN0M0	1	50/–	25	45
PatCA2	Hypopharynx, esophagus	cT4cN2M0	2	50.4/56	28	45
PatCA3	Larynx	pT1bN0M0	1	54/60	30	315
PatCA4	Hypopharynx	cT2cN2bM0	1	54/60	30	315
PatCA5	Nasopharynx	cT2cN2bM0	0	54/60	30	315
PatCA6	Larynx	pT2bpN1M0	3	50.4/56	28	45
PatCR1	Paranasal sinus	pT2cN0M0	1	50.4/61.6	28	270
PatCR2	Paranasal sinus	pT3N2bM0	0	54.4/64	32	0
PatCR3	Nasal cavity	cT3N0M0	1	50.4/56	28	90

For the nine investigated patients of this study, tumor site, TNM stage, dose prescription in the high and low dose PTV for the SIB treatment phase, number of SIB treatment fractions and time delay between rpCT and CBCT acquisition $\Delta t_{rpCT\text{-}CBCT}$ are given. The gantry angle of the generated SFUD plans is indicated, as well.

Supplementary Table II. OAR dose/volume constraints used during treatment planning.

	Dose/volume parameter	Tolerance dose (Gy)
Spinal cord	D_{max}	53
Brain stem	D_{max}	53
Parotids	D_{mean}	26
Optical nerves	D_{max}	54
Chiasm	D_{max}	56
Eyes	D_{max}	45
Eye lenses	D_{mean}	10

For the spinal cord, brain stem, optical nerves and chiasm, PRVs have been considered throughout this study. The optical nerves, chiasm, eyes and eye lenses constraints were only used for PatCR1–3, where these structures were delineated. The tolerance dose levels were chosen similar to the clinical values used for IMRT plan optimization at our institution.

Supplementary Table III. Gamma-index pass-rates for vCT- and $CBCT_{LUT}$-based dose recalculations.

	IMRT		IMPT	
	vCT (%)	$CBCT_{LUT}$ (%)	vCT (%)	$CBCT_{LUT}$ (%)
PatCA1	96	93	95	88
PatCA2	91	85	76	74
PatCA3	97	90	95	74
PatCA4	96	87	93	83
PatCA5	95	89	90	83
PatCA6	94	89	88	80
PatCR1	99	99	94	97
PatCR2	99	99	98	97
PatCR3	89	92	93	90

For each considered patient the vCT- and $CBCT_{LUT}$-based dose recalculation is compared to the rpCT-based recalculation by a (3%, 3 mm) 3D global gamma criterion.

Supplementary Table IV. BEV range pass-rates for vCT- and $CBCT_{LUT}$-based SFUD dose compared to the rpCT-based calculation.

	vCT (%)	$CBCT_{LUT}$ (%)
PatCA1	88	80
PatCA2	95	94
PatCA3	93	88
PatCA4	95	93
PatCA5	94	81
PatCA6	93	83
PatCR1	89	88
PatCR2	96	80
PatCR3	99	86

For each patient the vCT- and $CBCT_{LUT}$-based proton SFUD dose recalculation is compared to the rpCT-based recalculation in terms of the proton range in BEV. The depicted values indicate the amount of 1D profiles found within 3 mm of the rpCT.

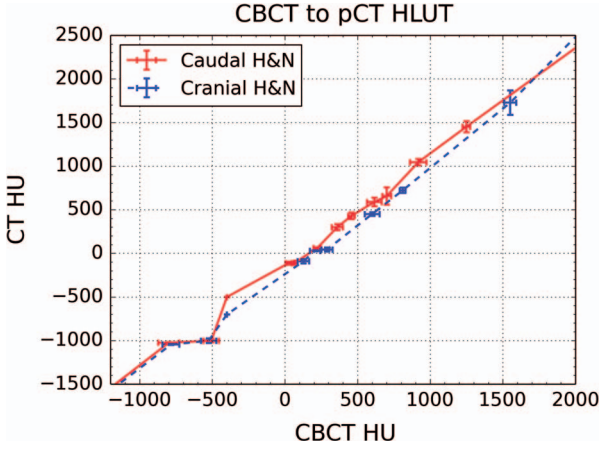

Supplementary Figure 1. HLUTs applied for intensity rescaling of the CBCT to the pCT. The two HLUTs used for patients with caudally (solid) and cranially located (dashed) lesions are depicted. Each data-point corresponds to a population average over multiple corresponding points in the registered pCT and CBCT in a narrow Hounsfield unit (HU) interval. The standard deviation at each point is indicated by error-bars.

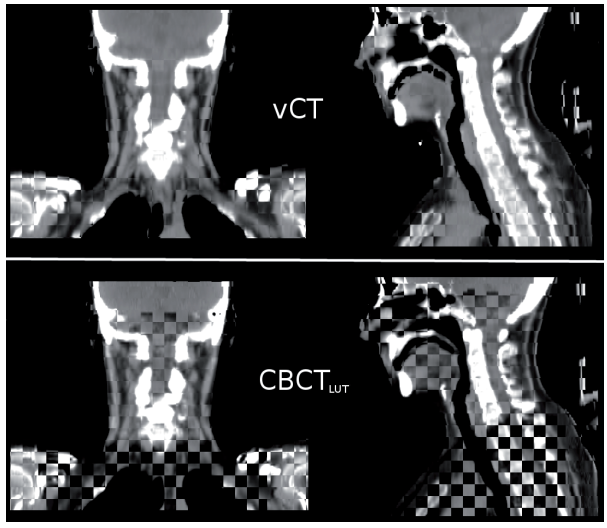

Supplementary Figure 2. Checkerboard display of vCT (upper row) and CBCT$_{LUT}$ (lower row) against the rpCT of PatCA2.

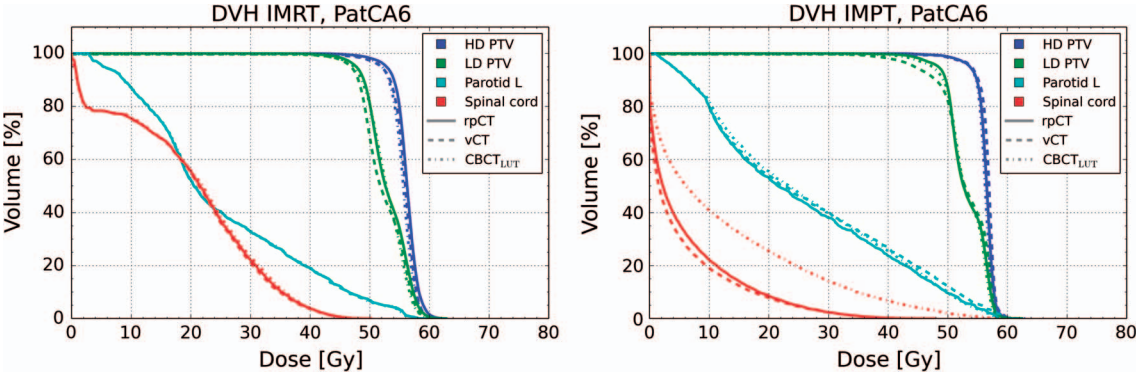

Supplementary Figure 3. DVH comparison of the IMRT (left) and IMPT (right) dose distributions of PatCA6 recalculated on the rpCT (solid line), vCT (dashed) and CBCT$_{LUT}$ (dotted). For improved visibility, only the high (HD) and low dose (LD) PTV (blue and green), as well as the left parotid (cyan) and the spinal cord (red) are depicted.

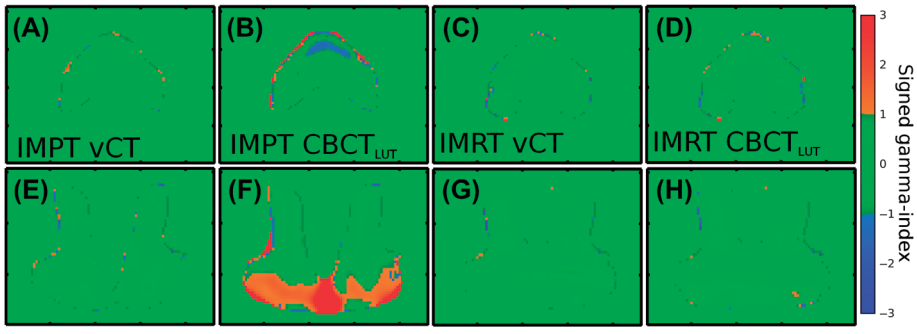

Supplementary Figure 4. Signed gamma-index displayed in a central axial (top row, A–D) and coronal slice (bottom row, E–H) for PatCA3. IMPT recalculations using the vCT (left column, A, E) and CBCT$_{LUT}$ (center-left column, B, F), as well as IMRT recalculations using the vCT (center-right column, C, G) and CBCT$_{LUT}$ (right column, D, H) are compared to the corresponding rpCT dose distribution.